International Journal of Chemical and Biochemical Sciences
(ISSN 2226-9614)

Journal Home page: www.iscientific.org/Journal.html

Wound Healing Activity of Pyrazole-thiazole Derivatives of Curcumin Through the Docking, Pharmacokinetics, MD Simulation and MM/GBSA Approaches

Md Shaekh Forid[1], Miah Roney[2], Md. Nazim Uddin[3], A. K. M. Moyeenul Huq[4], Mohd Hamzah Bin Mohd Nasir[5], Mohd Fadhlizil Fasihi Mohd Aluwi[2], Muhammad Saupi Azuri[1], Wan Maznah Binti Wan Ishak[1]*

[1] *Faculty of Chemical and Process Engineering Technology, Universiti Malaysia Pahang Al-Sultan Abdullah, Lebuhraya Persiaran Tun Khalil Yaakob, 26300, Gambang, Kuantan, Pahang, Malaysia.*
[2] *Faculty of Industrial Science and Technology, Universiti Malaysia Pahang Al-Sultan Abdullah, Lebuhraya Persiaran Tun Khalil Yaakob, 26300, Gambang, Kuantan, Pahang, Malaysia.*
[3] *Institute of Food Science and Technology, Bangladesh Council of Scientific and Industrial Research, Dhaka, Bangladesh*
[4] *Bio Aromatic Research Centre, Universiti Malaysia Pahang Al-Sultan Abdullah, Lebuhraya Persiaran Tun Khalil Yaakob, 26300, Gambang, Kuantan, Pahang, Malaysia.*
[5] *Bio Aromatic Research Centre, Universiti Malaysia Pahang Al-Sultan Abdullah, Lebuhraya Persiaran Tun Khalil Yaakob, 26300, Gambang, Kuantan, Pahang, Malaysia.*

Abstract

Matrix metalloproteinase (MMP-2 and MMP-8) have been found to be promising targets for the discovery and development for of novel wound healing drugs candidate. However, there are currently no MMP-2 or MMP-8 inhibitors that are therapeutically helpful for treating wound healing. Therefore, the goal of this study was to investigate the wound healing potential of novel pyrazole-thiazole derivatives of curcumin using a series of computational studies. We first utilized the physicochemical and ADMET to screen the eight curcumin analogs and the outcomes from showed that compound C2 is potential favorable compound for further exploration. The docking analysis showed that compound C2 has strong binding affinity with the MMP-2 and MMP-8 compared to reference drug. Furthermore, MD simulation result indicated C2/MMP-2 complex is more stable than C2/MMP-8 complex. Likewise, MM/GBSA results suggest that binding stability of C2/MMP-2 complex is more stable as they showed most negative binding free energy (ΔG_{bind} -24.434 kcal/mol) compared to C2/MMP-8 complex (ΔG_{bind} -12.347). Furthermore, PCA and FEL analysis revealed that C2/MMP-2 complex displayed stable complex formation compared to C2/MMP-8 complex in 100 ns molecular dynamics simulation trajectory. Hence, C2 could be considered a potent MMP-2 inhibitor and could be experimentally verified as a lead compound for the search for MMP-2 inhibitors for the treatment of wound healing.

Keywords: Curcumin, wound healing, matrix metalloproteinases, molecular docking, MD simulation.

Full length article **Corresponding Author*, e-mail: wanmaznah@ump.edu.my

1. Introduction

Wound healing is a multifactorial process that involves four consecutive phases that regulate wound healing, including hemostasis, inflammation, proliferation, and remodeling [1-2]. Any of these phases can be interrupted or run irregularly to cause a delay in healing or even nonhealing. By searched on the literature, it has been identified that the process of wound healing is connected to numerous proteins such as matrix metalloproteinases [3], vascular endothelial growth factor [4], tumor necrosis factor alpha, interleukin-1β [3], glycogen synthase kinase-3 beta [5]. However, the most important of these are matrix metalloproteinases (MMPs), named, MMP-2 and MMP-8 for wound heling. MMPs are zinc-dependent endopeptidases that are crucial in promoting cell migration and tissue remodeling,

essential for all wound healing phases [6]. MMPs are released by inflammatory cells the day after a wounding and cleanse the wound from damaged ECM and tissue [7]. Inflammation increases the level of protein including MMP-2 and MMP-8 [7].

MMP-2, also called gelatinases, are matrix metalloproteinases (MMPs) that play a role in collagen degradation and ECM remodeling [8]. A study demonstrated that MMP-2 is able to cleave gelatine as well as collagen types I and IV [9]. The activity of MMP-2 appears to be essential for a range of body functions, such as the formation and growth of new blood vessels, the repair of damaged tissues, and inflammation in wound healing. Researchers claimed that inhibition of MMP-2 accelerates diabetic wound healing by deducing inflammation, enhancing angiogenesis, and re-epithelializing the wound area. Furthermore, MMP-8 is another essential collagenase that plays a role in the breakdown of type I collagen and influences wound tissue repair [10-11]. An *in vivo* study concluded that overexpression of MMP-8 affects wound healing [11]. Another study revealed that the overexpression of MMP-8 was the primary cause of the increased collagenolytic characteristics of chronic wound ulcer secretions [12]. Overall, literature reported that the suppression of these proteins accelerates wound healing. Therefore, by considering data and earlier studies, MMP-2 and MMP-8 have been identified as potential targets for wound healing drug development.

Curcumin is a natural compound that has numerous biological activities and plays significant roles in the various stages of the wound healing process [5,13]. Consequently, several studies have reported that the derivatives of curcumin have significant anticancer efficacy [14]. It also inhibits several cell-signaling pathways, such as angiogenesis (vascular endothelial growth factor), proliferation (epidermal growth factor), inflammation (tumor necrosis factor; interleukin-1), and apoptosis [15]. Clinical researchers were additionally inspired to investigate the therapeutic potential of curcumin derivatives. A study reported that curcumin derivative-loaded nanofibers could have potential for diabetic wound healing (Alabdali et al., 2022). Researchers claimed that around 65 curcumin derivative clinical trials are currently being conducted globally targeting different diseases [16]. Likewise, several studies reported that curcumin derivatives could potentially prevent the generation of two key cytokines that are crucial for inflammation, such as interleukin-1 (IL-1) and tumor necrosis factor alpha (TNF-α), which are mainly responsible for wound site inflammation [17].

Recently, eight novel curcumin pyrazole-thiazole hybrids were reported (Figure 1) and tested for antiproliferative activity against different cell lines, and they reported antiproliferative activity against the growth of all tested cell lines [15]. However, no study has been reported on the wound-healing activity of these novel curcumin pyrazole-thiazole hybrids against the MMP-2 and MMP-8. Alternatively, the researcher claimed the curcumin derivatives have a beneficial effect on wound healing; thus, these novel curcumin pyrazole-thiazole derivatives were explored for their beneficial effects targeting the MMP-2 and MMP-8 proteins. The purpose of this investigation was to elucidate the wound healing potential of these derivatives by understanding their binding affinity with MMPs that are involved in the wound healing process using a series of computational approaches, including pharmacokinetic analysis, ADMET analysis, molecular docking, molecular dynamic simulation study, and finding free energy (MMP-GBSA).

2.Computational Methodology

2.1 Drug-likeness-based Screening

This test has to verify that the compounds meet these five specifications, also known as Lipinski's rule of five (MiLogP, molecular weight, hydrogen bond acceptor and donor, and topological polar surface area), in order to evaluate whether they have the chemical and physical properties needed to be used as a medication, particularly for oral intake by humans [18]. The bioactivity data of the compounds were investigated using the web-based server SwissADME (http://www.swissadme.ch/ index.php) [19]. To run the SwissADME tool, SMILES of compounds are necessary for training; comprehension of the active site or binding mechanism is not required; no previous understanding of the active site of proteins or the way of binding between targeted proteins and the compounds is essential.

2.2 ADMET-based screening

The ADME/T parameters are important for drug design and development. The ADMET profile could be used to evaluate the medicinal potential and safety of a product prior to its market release through investigating absorption, dispersion, metabolism, excretion, and toxicity [20]. In this study, the ADMET properties of the drugs and standard were analyzed using the previously published web program pkCSM (http://biosig. Unimelb.edu.au/pkcsm) in order to anticipate pharmacokinetic properties. In this current project, the ADMET properties of the drugs and standard were analyzed using the previously published web program pkCSM (http://biosig.unimelb.edu.au/pkcsm) in order to anticipate pharmacokinetic properties [21]. We explored absorption (aqueous solubility, human intestinal absorption), distribution (blood brain barrier), metabolism (CYP1A2 inhibitor; CYP2C19 inhibitor; CYP2C9 inhibitor; CYP2D6 inhibitor; CYP3A4 inhibitor; CYP2D6 substrate; CYP3A4 substrate), and toxicity (AMES toxicity; hERG II inhibitor; hERG I inhibitor; skin sensitization) through this in silico tools].

2.3 Molecular Docking

The docking analysis has been computed by utilizing the web-based docking program CB-Dock and the methodologies described before [22]. Four selected compounds named C1, C2, C7, and C8 from the ADMET-based screening were investigated to determine how they interacted with MMP proteins (MMP-2 and MMP-8). The structures Meanwhile, the target proteins' 3D structures have been retrieved from the Protein Data Bank (https://www.rcsb.org/) and downloaded in PDB format. Then for docking, a PBD file of the receptor and a.mol file of the compounds were uploaded into the CB-Dock application.

Throughout this approach, several top cavities were automatically selected and utilized for further analysis (cavity sorting), and molecular docking was performed at each one. After investigating the binding modalities, the docked position with the highest (1st posture) AutoDock Vina score and cavity size was chosen for further evaluation.

2.4 Molecular Dynamic Simulation

Molecular dynamic (MD) simulation investigation has been performed using the Desmond module of Schrödinger (Schrodinger Inc., USA) for checking the stability [23] of the docked complex structures of lead compound C2 with four MMP proteins (MMP2 and MMP-8). At first, the protein preparation wizard was used to start the simulation process as well as to optimize and minimize the complex structure utilizing the OPLS_2005 force field. Then, a buffer region of 10 Å was maintained between the protein atoms and the box's edges once the molecular system was enclosed in an orthorhombic box (10 Å× 10 Å× 10 Å). Further, transferable intermolecular potential-3-point (TIP3P) water molecules were used to solvate the system. Consequently, the system was neutralized by adding the appropriate positive (Na^+) and negative (Cl^-) ions, followed by the addition of 0.15 M NaCl. Also, the system was minimized for a 100 ns MD simulation using an NPT ensemble at 300 K temperature and 1.013 bar of pressure while keeping other settings to their default values and maintaining a convergence threshold and maximum iterations of 2000 [24]. Finally, a modeled system was loaded, and a MD simulation run up to 100 ns was conducted with a recording interval of 100 ps for total energy. The trajectories were examined to investigate the protein-ligand RMSD, ligand RMSF, protein-ligand RMSF, and protein-ligand contacts, respectively.

2.5 Binding free energy (MM/GBSA)

The relative binding free energies of docked complexes obtained during the 100 ns MD simulation were calculated using the molecular mechanics/generalized born surface area (MM/GBSA) method available in Maestro software [25-26]. The relative binding free energies values of docked complexes acquired during the 100 ns MD simulation were computed using the molecular mechanics/generalized born surface area (MM/GBSA) approach included in Maestro software. The approach had been adopted to investigate the lead C2 binding affinity for the proteins MMP-2 and MMP-8. These protein-ligand complexes were introduced into the OPLS-2005 force field, which estimated the binding free energy. The binding free energy was calculated, followed by the below equation. The binding free energy has been estimated, followed by the below equation.

$$\Delta Gbind = E_{complex} - E_{Protein} - E_{ligand}$$

Where, $\mathbf{E_{complex}}$ represents the free energy of minimized protein-ligand complex, $\mathbf{E_{protein}}$ is the free energy of minimized protein only, while $\mathbf{E_{ligand}}$ is the free energy of minimized ligand.

2.6 Principal Component Analysis and Free energy landscape analysis

The analytical methods principal component analysis (PCA), also known as the essential dynamics (ED) is widely used to illustrate the slow and functional movements and conformational changes of biomolecules from simulation trajectories [27]. The PCA was constructed by following to the previously published, comprehensive mathematical description [28]. The GROMACS analysis tool, GROMACS inbuilt modules g_covar & g_anaeig were engaged to perform PCA of four complexes (MMP-2/C2 and MMP-8/C2) as per as trajectories obtained from 100ns MD simulation [29]. For PCA, initially construction of diagonal covariance matrix from Ca atom of the protein (MMP-2/C2 and MMP-8/C2) was carried out that captures strenuous motion of the atom through eigenvectors and eigenvalues. The eigenvalue and eigenvectors for the covariance matrix were diagonalized and solved to get the major components of the proteins. The direction of motion is represented by the eigenvectors, while the amplitude and direction of motion are represented by the eigenvalues [30]. The first two PCs accounted for more than 80% of the overall position fluctuation which was evaluated by ED analysis for the demonstration of protein's motion [30-31]. However, to clarify the conformational behavior pattern of each complex first two eigen- vectors (eigenvectors 1 and 2) were used to make a 2D projection of each of the independent trajectories. Furthermore, FEL analysis was executed using first two principal components, PC1 and PC2 using gmx_sham module of GROMACS to identify energetic structural changes and to visualize the energy minima during 100ns simulation [27]. Free energy landscape (FEL) is a representation of possible conformation taken by a protein in molecular dynamics simulation along with the free energy minima [32]. FEL is a representation of two variables that quantify conformational variability and reflect certain system attributes [33].

3. Results and Discussion

3.1 Drug-likeness-based Screening

To become an orally active drug, it is important for a substance to comply with a number of physicochemical parameters as described by Lipinski's rule of five [18]. The following criteria can be used to identify the properties of a medication that are similar to those of other drugs such as molecular weight, hydrogen bond donors and acceptors, topological polar surface area, and consensus (Log Po/w) [34]. The molecular weight should be between 150 to 500 g/mol, and there should be no more than five and no more than ten hydrogen bond donors and acceptors, respectively [35]. The allowed range for Log Po/w cannot be higher than 6.00, whereas the value of TPSA must be between 75 $Å^2$ to 140 $Å^2$ [36].

Lipophilicity of drug candidate molecules is a key characteristic for the development of their dosage form because drug molecules must cross most biological membranes' lipid bilayer [35]. As shown in Figure 2, all the compounds demonstrated the expected lipophilicity. However, all the derivatives of curcumin showed slightly

poor solubility, which can be overcome by forming nanoparticles. The physiochemical properties of selected compounds are shown in Table 1. From the results, it has been shown that the molecular weight (523.60-602.50) of the selected compounds is higher compared to the standard drugs; however, this could be in an acceptable range excluding the C8 compound, which is higher. Likewise, hydrogen bond donors (02-03) and acceptors (06-08), topological polar surface area (117.87 Å² to 163.69 Å²), Log Po/w (4.96 to 5.85), which all fall within standard ranges, The Lipinski rule was applied to precisely anticipate the drug likeness, and all the selected compounds complied with it. Therefore, it has been predicted that they could be utilized as medicines.

3.2 ADMET-based screening

Virtually every aspect of drug research and development is being simulated, and decision-making is assisted by computational or *in silico* methodologies [20]. Computer-aided drug discovery (CADD) methods are gaining interest since they can help reduce the scale, time, and cost problems associated with traditional experimental methods since used as the primary assessment of compounds for ADME-Tox properties in order to identify drug candidates with high potency and low toxicity [37]. The *in-silico* investigation could be used to determine the drug-likeliness of a compound using the ADMET, Distribution, Metabolism, Excretion and toxicological properties [38]. ADMET screening has been utilized to predict the pharmacokinetic behavior of curcumin pyrazole-thiazole compounds when delivered to and eliminated from the circulatory system. Based on the outcome of the pkCSM web server, Table 2 represents the ADMET results of eight pyrazole-thiazole derivatives of curcumin. Table 2 summarizes the ADMET findings of eight pyrazole-thiazole derivatives of curcumin based on the results of the pkCSM web server. According to the results, It was anticipated that each of the compounds would be able to be easily absorbed in the human gut, and they all showed encouraging logarithms of molar solubility values that ranged from -4.421 to -3.713. All of the compounds demonstrated moderate to excellent absorption (89.38–100%). Moreover, compounds C2, C3, and C6 showed the highest absorption, which was 100%, indicating that this compound has excellent absorption compared with the reference drug gentamicin (19.16%). The blood-brain barrier has a moderate distribution (-1.146 to -1.706) of all substances compared with the reference drug.

Drug metabolism is a term that is frequently used to explain how pharmaceutical drugs undergo biosynthesis inside the body. Some different types of enzymatic substrates are produced due to drug metabolism, and each one possesses its pharmacokinetic, physicochemical, and pharmacological properties. Thus, it is of utmost significance to consider how the medication will be metabolized and how it will interact with other prescription medications. Based on the results, it showed that none of the selected substances inhibited CYP2D6. CYP2D6 is the second-most studied drug-metabolizing enzyme. It has been claimed that about 75% of the marketed medicine is metabolized by CYPs, with the five major CYP isoforms representing 75–90% of CYP-related metabolism [39]. From the results, it has been concluded that all of the agonists were confirmed to effectively substrate CYP450, CYP2D6 and CYP1A2, which implies that they might all be easily oxidized and hydroxylated in the initial phases of metabolism. Furthermore, AMES's toxicity is evaluated using its carcinogenicity to confirm that the expected chemicals are not hepatotoxic, skin-sensitizing, or carcinogenic. Following our prediction, none of the ligands might be carcinogenic. However, all the ligands are free of skin sensitization effects, although ligands C3, C4, C5, and C6 may have a hepatotoxic effect, while other substances do not show a hepatotoxic profile. Thus, it was established that compounds C1, C2, C7, and C8 posed no danger of liver damage. Additionally, the chosen chemicals do not affect skin sensitization. Additionally, human intestinal absorption was considered for screening the compound, and it was found that C2 absorption is high compared to C1, C7, and C8. From ADMET analysis, these compounds could be favorable medications. Therefore, C2 was selected for further study for molecular docking and molecular dynamic simulation to confirm the binding affinity with the proteins.

3.3 Molecular Docking

To explore the molecular interaction approach and gather information on the ligand's ability to bind to the target protein and inhibit it, docking investigation modeling was carried out. The CB-Dock program was utilized to screening four compounds from the ADMET-based screening for docking-based screening [40-41]. The screening revealed a wide range of binding affinities for both target proteins. Finally, the most promising candidate for inhibiting the target protein interaction was chosen for future investigation.

3.3.1 Docking interaction with the MMP-2

The docking simulation of hit compounds C2 and Gentamicin (reference) into MMP-2 (PDB ID: 1GEN) was visualized and analyzed, as shown in Figure 3 and Table 3. It has been found that C2 interacts with a variety of MMP-2 amino acid residues and forms seven hydrogen bonds and six hydrophobic interactions with different residues of amino acid with a binding interaction value of -8.2 kcal/mol. Similarly, gentamicin interacted with eleven hydrogen bonds and six hydrophobic bonds with different residues of amino acids, with a binding interaction value of -7.0 kcal/mol. These findings indicated that C2 showed more potential binding affinity than reference.

3.3.2 Docking interaction with the MMP-8

The hit compound C2 was docked into the protein MMP-8 (PDB ID: 5H8X) binding site in the current investigation (Figure 4). The reference compound, Gentamicin, interacted with nine hydrophobic interactions and seven hydrogen bonds with a binding interaction value of -7.2 kcal/mol (Table 4). However, the compound C2 interacted with six hydrogen bond and seven hydrophobic bonds with a binding energy of -7.8 kcal/mol, indicating low binding energy, which was comparable to the reference compound (Table 4). The favourable docking affinity suggests strong binding of C2 within the binding cavity of the MMP-8.

3.4 Molecule dynamics (MD) simulation analysis

In this study, the MD simulation was conducted to determine the dynamic interactions and to gain a deeper understanding of the stability of each protein-ligand complex during the 100 ns MD simulation. Nowadays, MD simulation is an expanding and widely used tool for evaluating conformational changes and binding affinities of protein-ligand complexes in the drug design and discovery fields [42-43]. A number of parameters, including root-mean square deviation (RMSD), root-mean square fluctuation (RMSF), protein–ligand contacts mapping, and hydrogen bond interaction, were calculated from 100ns MD trajectories to investigate their structural stabilities, binding modes, and binding strengths. The RMSD value was calculated over time and shown in Figure 5 for C2/MMP-2 and C2/MMP-8 systems to evaluate the stability of docking complexes. The low fluctuations of the simulated system are indicated by the small RMSD values, indicating the stability of the docking complex [44]. Figure 5 shows that compound C2 is bound with MMP-2 and MMP-8. Monitoring the RMSD value of both complexes, the structural conformation of MMP-2 and MMP-8 remain stable when bound with compound C2; however, lower fluctuation may not significantly affect its overall conformational changes in their bound states. Figure 5A demonstrated that RMSD of Cα atoms is stable in a range of 1.33 and 3.0 Å while the ligand atoms fluctuated to 9.7 Å during the first period before stabilizing in a range of 1.8–9.7 Å (Figure 5A). Moreover, in the C2/MMP-8 complex, the protein MMP-8 and ligand C2 RMSD were in the range of 0.9–3.3 Å and 0.9–8.9 Å, respectively (Figure 5B). Overall, the RMSD values of all the complexes were in an acceptable range. Therefore, the compound may effectively bind to the active sites of the targeted proteins MMP-2 and MMP-8. RMSF plot shows the fluctuation of individual residues of MMP-2 and MMP-8 proteins (Figure 6). Vertical green lines on the X-axis show the point of contact of the C2 with the protein residue. From the RMSF plot analysis for C2/MMP-2, the 82-85 and 161-165 residues fluctuated more than others but were not out of the range (Figure 6A). Important amino acid residue for the interaction has been found in Asn 573, Ser,575, Lys576, Asp 622, Leu 623, Gln624, Gly625 and Gly626 (Figure 6A). Similarly, figure 6B shows that the residues from 67-72 and 76-82 fluctuated more than those within an acceptable range. C2/MMP-8 RMSF plot demonstrated that His147, Gly148, Asp149, Asn150, Ser151, Pro152, Pro156, Asn157, Gly158, Ile159, Leu160, Ala161 and His162 are responsible for the fluctuation.

The protein-ligand contact of the C2/MMP-2 complex is shown in Figure 7. The bar graph showed that the hydrogens generated by Glu 530 and Gln 625 are the highest in percentage and show more stable interactions. Also, the hydrophobic interactions generated by Arg 482, Pro 527, and Lys 558 are identified. In addition, ionic interaction was found to be highest identified in Glu 525 (Figure 7A). Figure 8A showed that Glu 525 and Glu 530 showed 65% and 95% hydrogen bonding, and Gln 625 was responsible for hydrophobic bonding, respectively (Figure 8A), and some residues have more than one specific interaction with the ligand, which is highlighted by a darker orange color (Figure 9A). Moreover, the C2/MMP-8 complex shows that the hydrogens are generated by Asp149, Asn150, Ser151, Asn188, His197, Tyr216, Pro217, And Ala220 (Figure 7B). However, among several hydrogen bonds, Asn218 had the highest percentage, while Pro152 and His197 had the highest hydrophobic bond interactions (Figure 8B). The ligand-atom interaction diagram showed that C2 could form an H-B bond interacting with His197 in the benzene ring and a hydrophobic bond with Ile159 (Figure 9B). Additionally, some residues have more than one interaction with the ligand, indicated by a darker orange (Figure 9B).

3.5 Binding free energy analysis (MM/GBSA)

The binding free energy (ΔGBind) was calculated using the most accurate technique, MM/GBSA, to investigate the binding affinity of C12 from the MD simulation trajectories. According to Table 5, both complexes exhibited negative MM-GBSA binding energy, indicating favorable interactions. Additionally, Table 5 includes MM/GBSA profile data, including Coulomb energy, hydrogen-bonding correction, Pi-pi packing correction, lipophilic energy and van der Waals energy. The average ΔGBind of C2/MMP-3 and C2/MMP-8 was found to be -24.43 and -12.34 kcal/mol respectively, which suggests that both proteins have a strong complex with Compound C2.

3.6 Principal Component Analysis & Free energy landscape analysis

Principal component analysis (PCA) was used to further assess the conformational changes in MMP-2 and MMP-8 following their binding to C2 during the MD simulation [45]. Plots of the eigenvalues derived from the diagonalization of the covariance matrix of the Cα atomic fluctuations are shown in Figures 10A and 11A. The eigenvalue amplitude decreases, suggesting a change from coordinated movements to more confined, localised oscillations. The results of this study indicated that a larger proportion of the total movements in all simulations may be explained by the first two eigenvectors that were derived via PCA. The motion characteristics for MMP-2 and MMP-8 reported by the first two PCs were slightly different, as can be shown in Figures 10A and 11A, respectively.

Using projections of MD trajectories on the first two PCs, the conformational spaces of MMP-2 and MMP-8 were created in order to get important information on the structural changes of these proteins in the free state. In addition, the displacements of eigenvectors 1 and 2 were computed in order to gain a deeper understanding of the movements (Figure 10B and 11B). The overall motion of the MMP-2 and MMP-8 proteins has distinct subspaces of structures during 100-ns MD simulations, particularly in PC1 mode, as seen in Figures 10B and 11B. The proteins in PC1 visit four conformational clusters, as shown by Figures 10B and 11B. Based on the MMP-2 root-mean-square fluctuation (RMSF) analysis of PC1, these clusters are associated with increased displacements in the residue areas of 130–135, 150–153, 167–170, and 180–192 (Figure 10C). Additionally, these clusters correlate to elevated displacements in the areas of 62-73, 75-82, 87-94, and 125-160 residues, according to the RMSF analysis of PC1 for MMP-8 (Figure 11C).

Two porcupine plots, which use the first and second eigenvectors using GROMACS software, are shown in Figures 10D and 11D to examine the variations in the motion behaviors in the PC1 and PC2 modes. The arrow's length

indicates the force of the motions, and its direction indicates the direction of the collective motion. The conformation of free MMP-2 and MMP-8 differs from that of the proteins' MMP-2/C2 and MMP-8/C2 complexes, as shown by these figures.

The projections of their respective first (PC1) and second (PC2) eigenvectors were used to build the free energy landscape (FEL) values of MMP-2 and MMP-8, which allowed for the determination of the low-energy basins (minima) and the stability of the protein investigated throughout the simulation (Figure 10E and 11E). Dark blue colors suggest energy minima and energetically favored protein conformations, whereas red colors indicate unfavorable conformations. MMP-2 and MMP-8 protein stability was demonstrated by the simulation's shallow and narrow energy basin. These Figures indicated that MMP-8 displayed a cluster of two linked energy minima basins close to one another (Figure 11E) and MMP-2 displayed a cluster of one connected energy minima basin close (Figure 10E).

4.0 Discussions

Wound healing is a complex process and, at the same time dynamic in nature, comprising a sequence of various phases occurring within a specific time frame. The number of patients suffering from wound healing is increasing worldwide and placing a significant burden on individuals and healthcare systems. Similarly, treating chronic wounds remains an important concern for the medical system [46]. Wound healing is associated with many proteins responsible for regulating this complex physiology. Among several protein me matrix metalloproteinases (MMPs) play a vital role in the restoration of damaged skin by modifying the wound matrix, thus enabling cell migration and tissue remodeling, which is crucial for wound re-epithelialization [10]. During wound healing, the expression and activity of different MMPs are precisely regulated [10]. Through mediating various cellular events such as angiogenesis and vasodilation, MMPs are crucial for wound healing.

Researcher reported that MMP-2 are responsible for cell fibroblast migration during angiogenesis and play an ECM remodeling in wound healing [8]. According to Caley et al. (2015), MMP-2 regulates angiogenesis during wound healing by activating proangiogenic cytokines including TNF- and VEGF and producing antiangiogenic peptides [10]. Additionally, MMP2 has been found to be involved in various physiological and pathological processes, such as wound healing, cancer metastasis, and tissue regeneration [47]. On the other hand, Study reported that MMP-3 is crucial for the degradation of collagens as well as proteoglycans, laminin, and fibronectin [10,48]. Another *in vitro* and in vitro study reported that MMP-3 induced the proliferation, migration, and survival (antiapoptosis) of endothelium and accelerated angiogenesis and pulp wound healing [49]. Moreover, MMP-8 is another essential collagenase is played a role to breakdown of type I collagen and influence in wound tissue repair [10-11]. The above finding suggesting the importance of MMP2 and MMP-8 for angiogenesis and tissue remodeling. Several studies were reported conducted but targeting these four important proteins is still not sufficient. Therefore, in this study these four important MMPs was targeted to conduct the study.

Natural products in the treatment of wounds have been reported in numerous studies and reported to have beneficial effects such as antioxidant, anti-inflammatory, and antimicrobial properties, which can also interact in the various stages of the wound healing process [50]. Among several natural products, curcumin's beneficial effect is crucial for different treatments. Research has reported that curcumin can potentially reduce inflammatory activities and promote proliferation and tissue remodeling in wound healing [51]. Another study reported that curcumin enhances wound healing by inhibiting the inflammatory response [52]. Consequently, studies have reported that curcumin derivatives have antibacterial activity against drug-sensitive microbes such as *Staphylococcus aureus, Salmonella enterica, Enterococcus faecalis, and Escherichia coli*, which are frequently found in chronic wound areas [5]. Palabindela et al. (2023) reported that curcumin-based pyrazole-thiazole derivatives have potential as antiproliferative agents [15]. However, these novel pyrazole-thiazole derivatives have not yet been described in the literature as potential wound healing agents. Thus, this study was designed to find out the potential wound healing targets of MMP-2, and MMP-8. For this reason, pharmacokinetics, ADMET, molecular docking, molecular dynamic simulation, and MMGBSA analysis were conducted using an in-silico approach.

The drug-likeness-based Screening and physicochemical parameters as described by Lipinski's rule of five, were analyzed using SwissADME, a popular web-based tool. The finding suspected that all the selected compounds complied with it (Table 1) and predicted that they could be utilized as medicines. However, all the curcumin derivatives showed slightly poor solubility, which can be overcome by forming nanoparticles. Additionally, all the compounds demonstrated the expected lipophilicity (Figure 2).

Computational techniques and prediction of the various physicochemical and pharmacokinetic properties of novel drug candidates are one of the ways of the drug development process that can save time, effort, and cost [53]. Computer-aided drug discovery (CADD) methods are currently gaining popularity because they can help reduce the scale, time, and cost problems associated with traditional experimental methods when used as the primary evaluation of compounds for ADME-Tox properties to find drug candidates with high potency and low toxicity [37]. Therefore, the pharmacokinetic behavior of eight pyrazole-thiazole derivatives of curcumin was predicted using ADMET screening analysis using the pkCSM web server. The findings suggest that C2, C3, and C6 showed the highest absorption among the eight compounds. Then, the metabolism and toxicity behavior of the compounds were analyzed which showed that compounds C1, C2, C7, and C8 are safe for use. Then, the human intestinal absorption was considered for screening the compound, and it was found that C2 absorption is high compared to C1, C7, and C8 (Table 2). Thus, the compound C2 was selected for further study for molecular docking and molecular dynamic simulation to predict the binding affinity of protein ligands.

Molecular docking is a vital tool in new drug design and development, it predicts the mechanism of binding mode and conformation of novel compounds within the binding pocket of protein target [54].

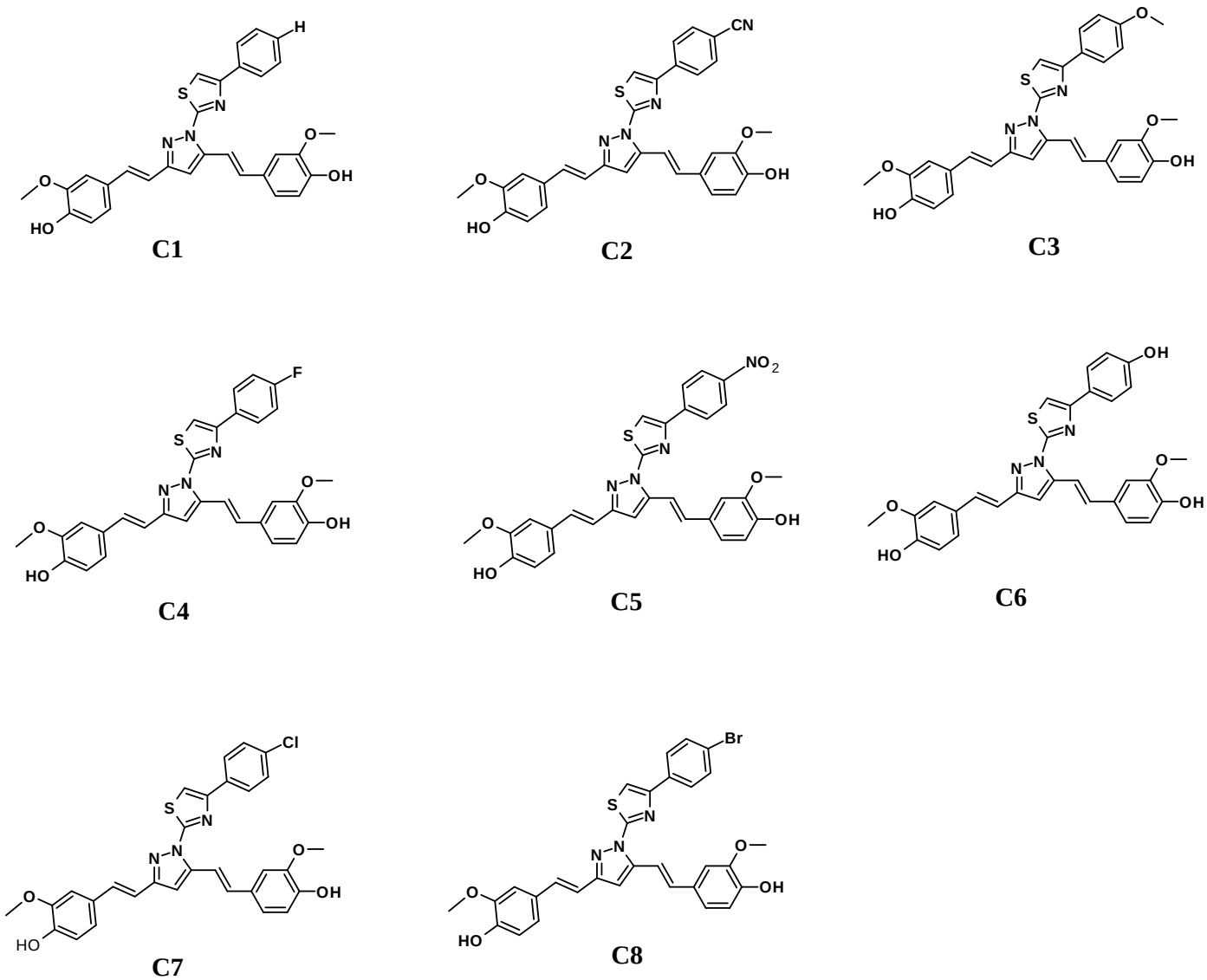

Figure 1. Pyrazole-thiazole derivatives of curcumin [15]

Table 1: Determination of the physicochemical properties of the selected compounds (C1-C8).

Compound	MW (g/mol)	Log (S)	No. RB	No. HBA	No HBD	TPSA (Å^2)	Consensus Log $P_{o/w}$	Lipinski rule	
								Violation	Violation parameter
GM	477.60	0.24	7	12	8	199.73	-2.15	03	HBA,HBD,TPSA
C1	523.60	-7.36	8	6	2	117.87	5.54	01	MW>500
C2	548.61	-7.31	8	7	2	141.66	5.35	01	MW>500
C3	553.63	-7.44	9	7	2	127.10	5.55	01	MW>500
C4	541.60	-7.52	8	7	2	117.87	5.85	01	MW>500
C5	568.61	-7.43	9	8	2	163.69	4.96	01	MW>500
C6	539.60	-7.23	8	7	3	138.10	5.12	01	MW>500
C7	558.05	-7.96	8	6	2	117.87	6.07	01	MW>500
C8	602.50	-8.27	8	6	2	117.87	6.18	01	MW>500

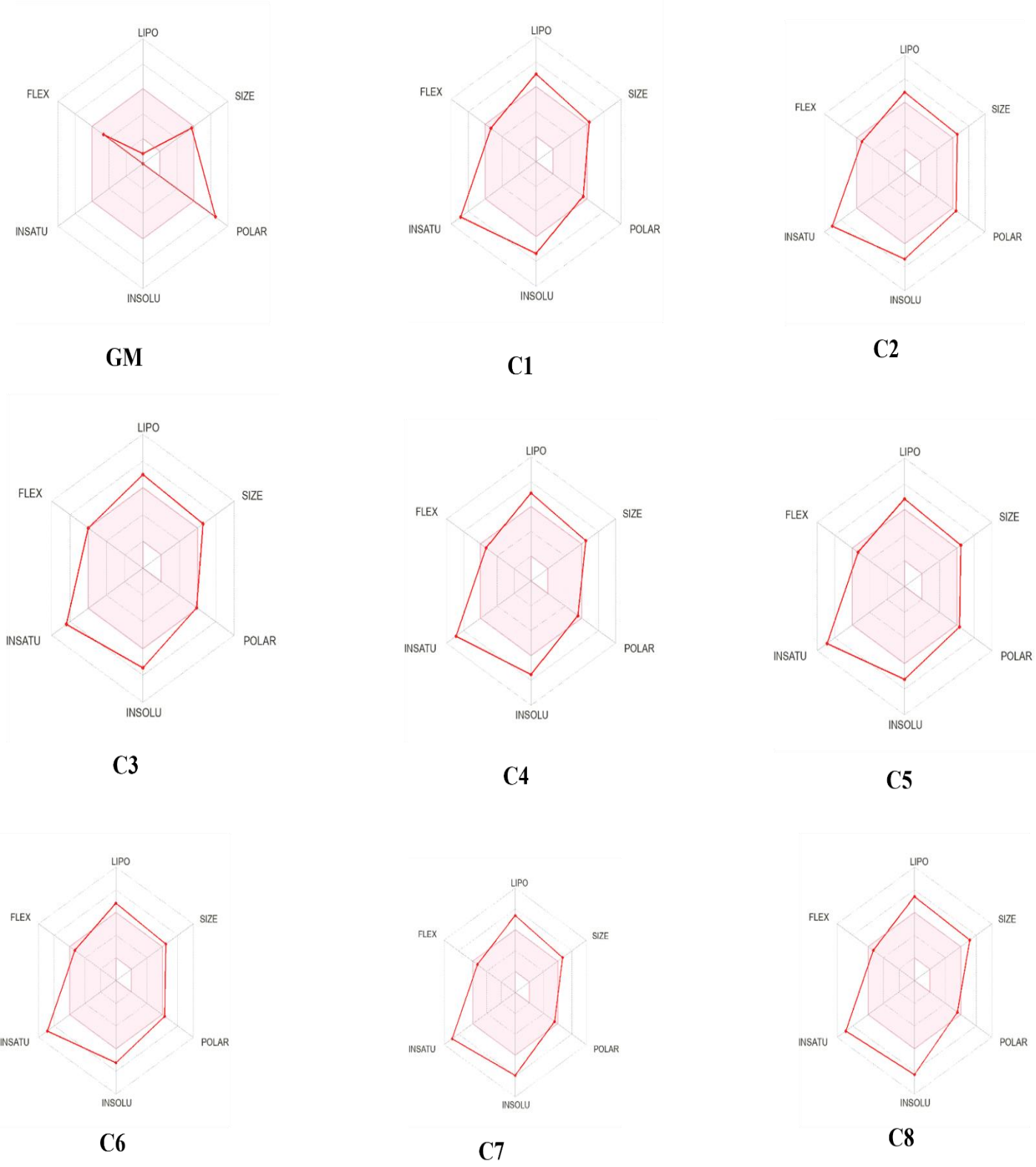

Figure 2: Prediction of the physicochemical characteristics of the pyrazole-thiazole derivatives of curcumin (C1-C8). (Lipophilicity: LIPO; Insolubility: INSOLU; Instauration: INSATU; Flexibility: FLEX; Polarity: POLAR)

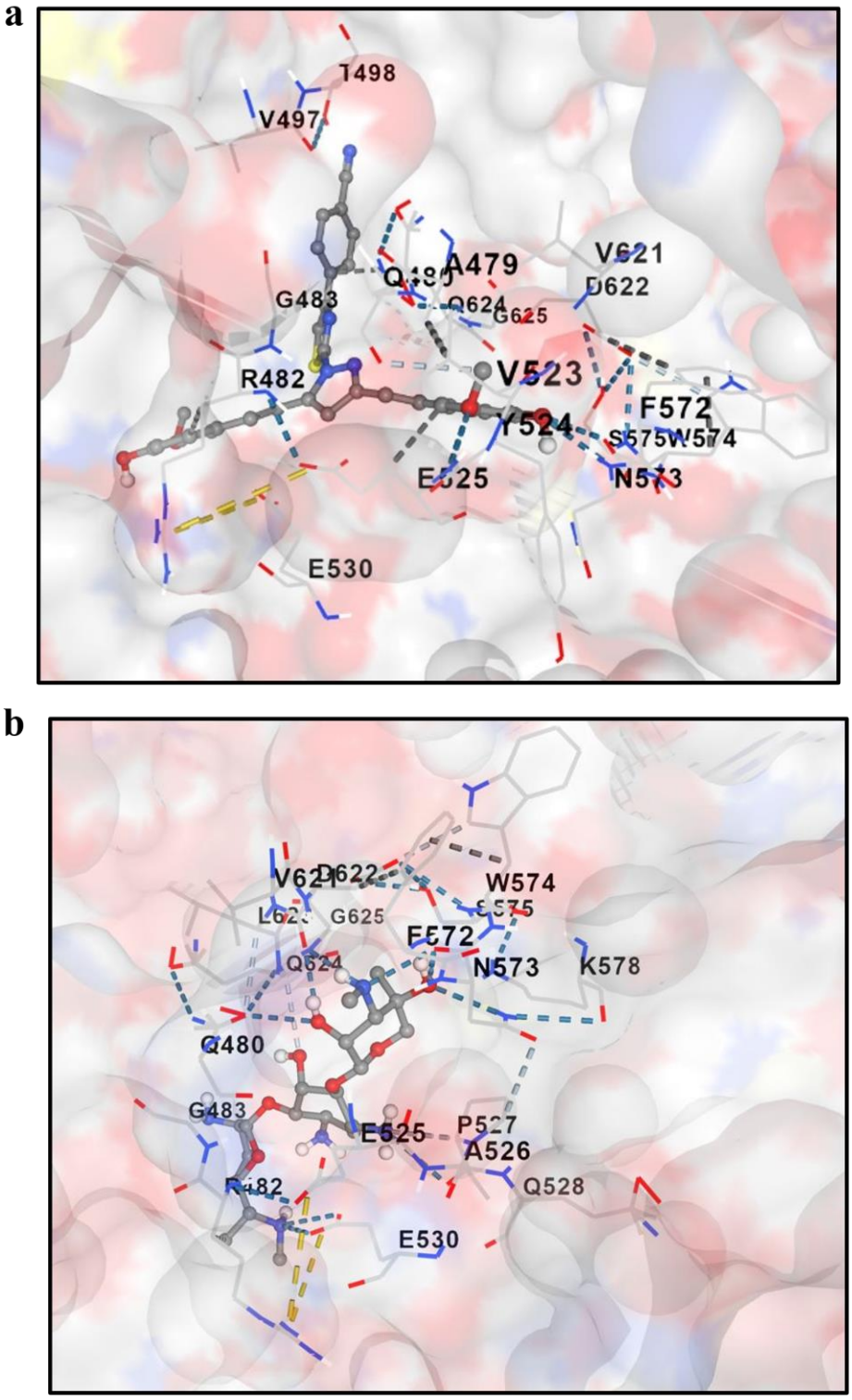

Figure 3: Molecular docking of MMP-2 with (a) C2 and (b) reference drug

Table 2: Summary of *in silico* ADMET prediction of pyrazole-thiazole derivatives of curcumin (C1-C8).

---	Absorption		Distribution	Metabolism							Toxicity			
CN	WS (Log S)	HIA (%)	BBB	CYP2D6 substrate	CYP3A4 substrate	CYP1A2 inhibitior	CYP2C19 inhibitior	CYP2C9 inhibitior	CYP2D6 inhibitior	CYP3A4 inhibitior	AMES toxicity	hERGI inhibitor	Skin sensitization	HT
Reference Value	---	70-100 %	---	No	No	No	No	No	No	No	No	No	No	No
GM	-2.843	19.16	-0.851	No	No	No	No	No	No	No	No	No	No	No
C1	-4.412	89.38	-1.146	No	Yes	No	Yes	Yes	No	Yes	No	No	No	No
C2	-4.35	100	-1.333	No	Yes	No	Yes	Yes	No	Yes	No	No	No	No
C3	-3.964	100	-1.397	No	Yes	No	Yes	Yes	No	Yes	No	No	No	Yes
C4	-3.931	89.68	-1.368	No	Yes	No	Yes	Yes	No	Yes	No	No	No	Yes
C5	-4.096	99.40	-1.537	No	Yes	No	Yes	Yes	No	Yes	No	No	No	Yes
C6	-3.713	100	-1.706	No	Yes	No	Yes	Yes	No	Yes	No	No	No	Yes
C7	-4.419	88.58	-1.335	No	Yes	No	Yes	Yes	No	Yes	No	No	No	No
C8	-4.421	88.52	-1.344	No	Yes	No	Yes	Yes	No	Yes	No	No	No	No

Table 3: Predicted results of docking with the MMP-2 with C2 compound and standard

Compound	**Vina score**	**Cavity size**	**Bound amino acids**	
			H-B interaction	**Hy-B interaction**
GM	-7.5	175	LYS578,ASN573,SER575, ASP622, GLN480,GLU484,GLN624, GLU525,GLU530,PRO527, GLN480	PHE572, LYS578, PRO527
C2	-8.2	143	LYS578,ASN573,GLN528, PRO527,GLN480,GLN624, VAL497	ASN573,PHE572,TYR524, VAL621, GLN480, GLN624
Note: *H-B : Hydrogen bond; Hy-B: Hydrophobic bond*				

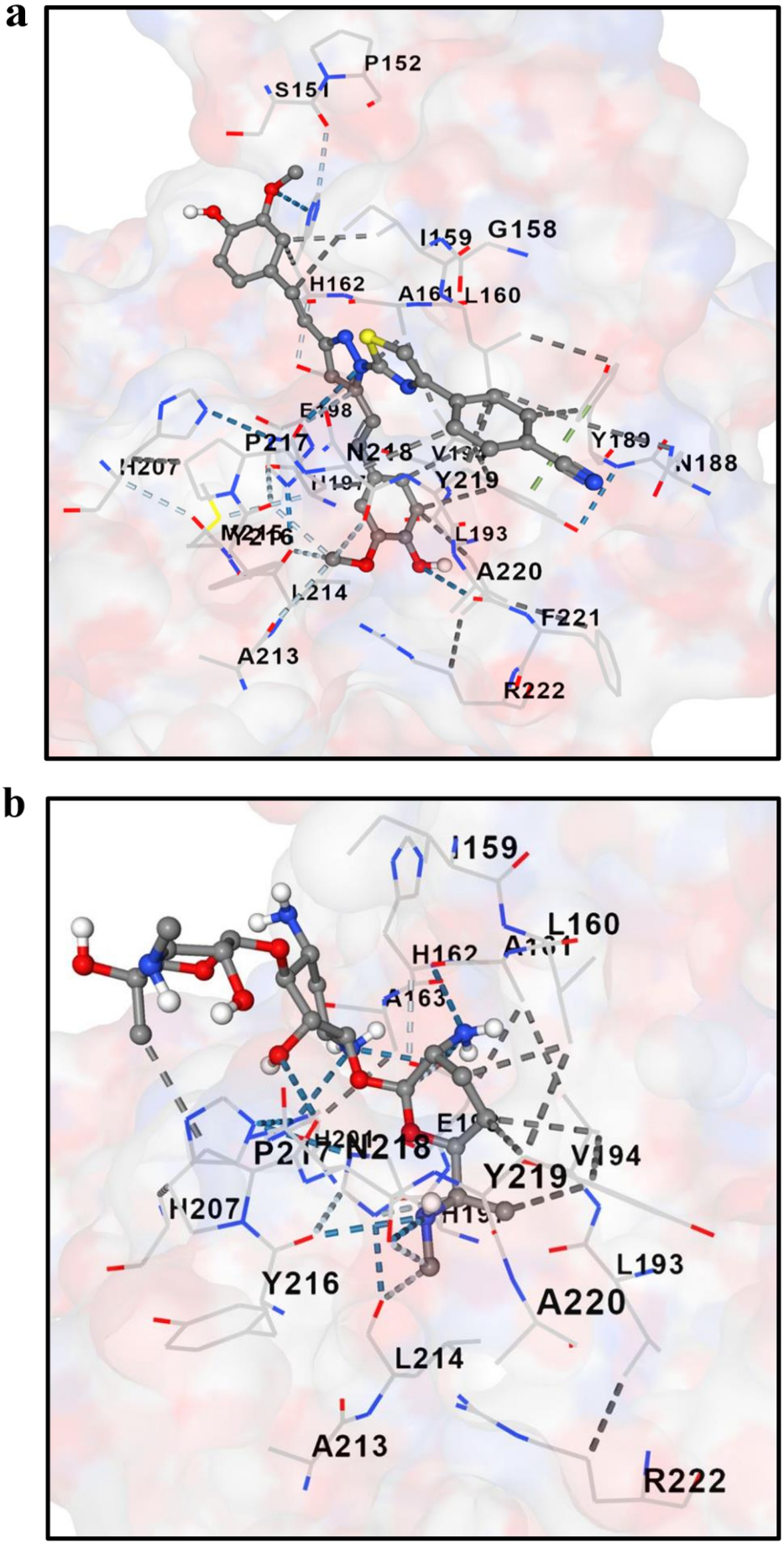

Figure 4. Molecular docking of protein MMP-8 with (a) C2 and (b) reference drug Gentamicin

Table 4: Predicted results of docking with the protein MMP-8 with compound C2 and Gentamicin (standard).

Compound	Vina score	Cavity size	Bound amino acids	
			H-B interaction	Hy-B interaction
GM	-7.2	375	Ala161,Glu198,Pro217,His207, Tyr216, Leu214, Asn218	Pro217, His207, Leu193, Tyr219, Val194, Leu160, Ala161
C2	-7.8	226	Leu214, Tyr216, Pro217, His207, His197, Asn85	Val194, His197, Ala161, Ala163, Ile159, His207, Leu160
Note: *H-B: Hydrogen bond; Hy-B: Hydrophobic bond*				

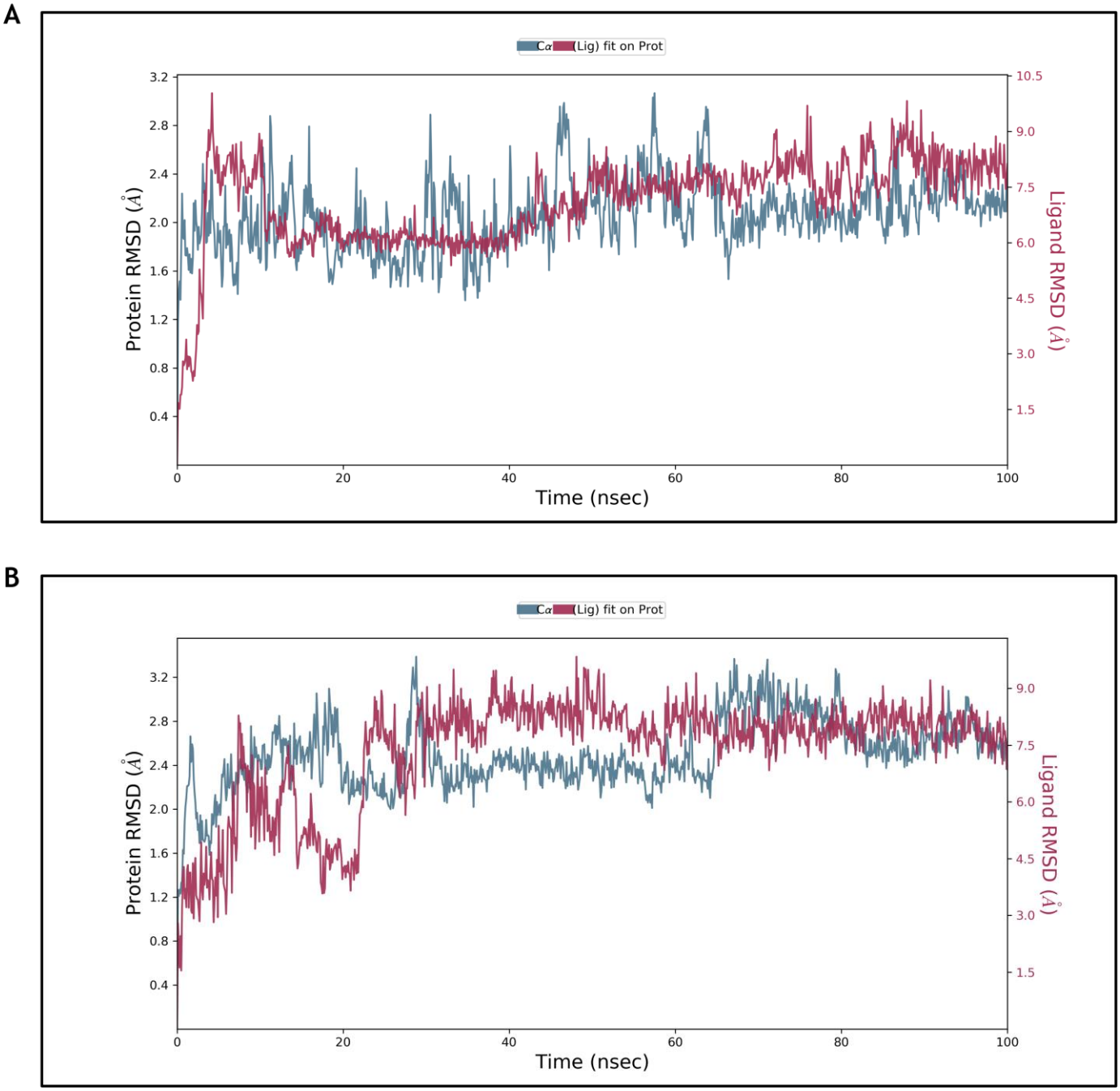

Figure 5. RMSD vs time plots of Protein-ligand complexes in MD simulations study. (A) C/MMP-2 complex (B) C2/MMP-8 . Protein showed as blue line and compound as red line. (*The reader is guided to the Online version of this paper for explanation and interpretation*).

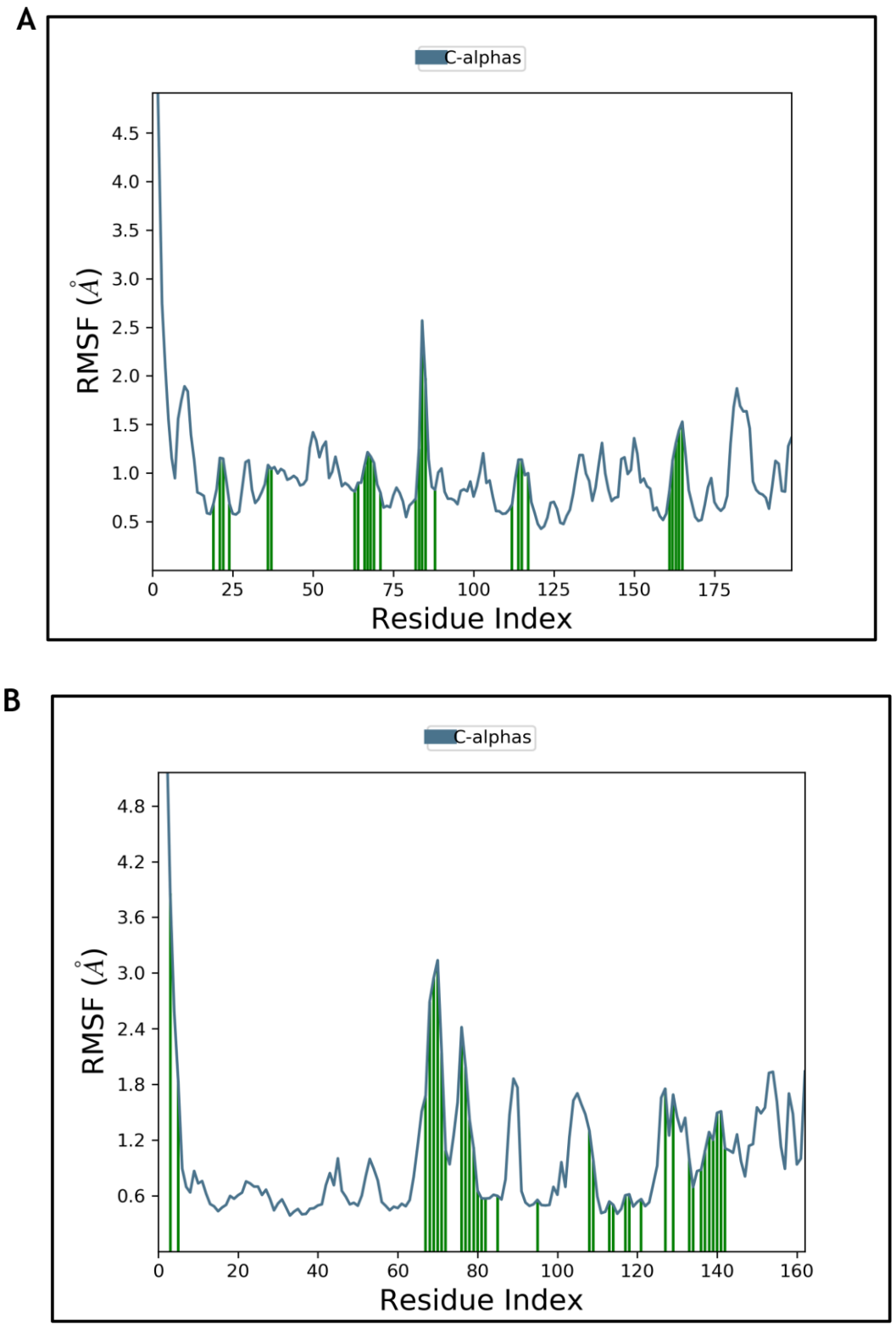

Figure 6: RMSF plots of Proteins. (A) MMP-2 and (B) MMP-8 with respect to hit compound C2.

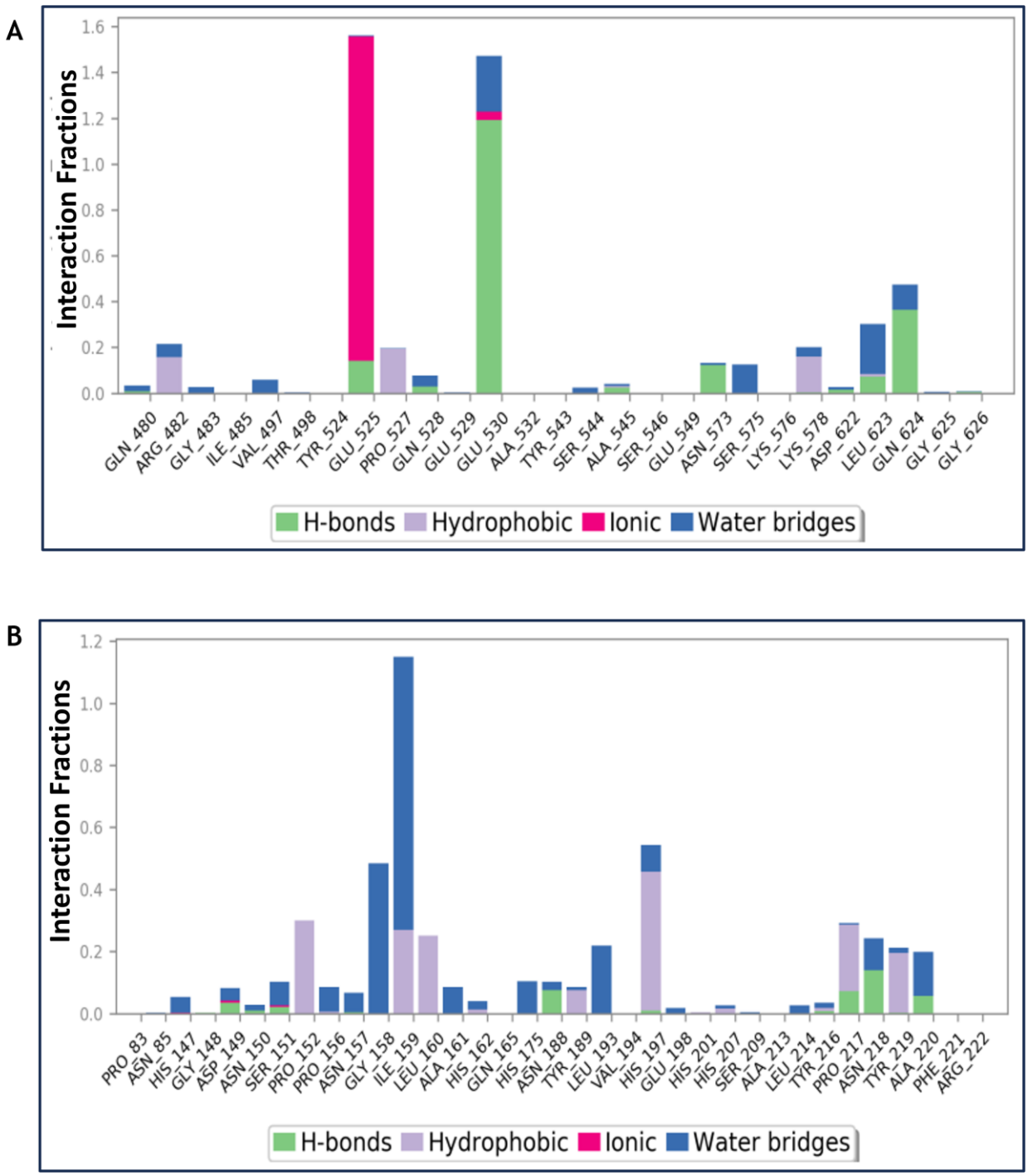

Figure 7: Protein–ligand contacts during MD simulations study. (A) Protein MMP-2 and compound C2 (C) Protein MMP-8 and compound C2.

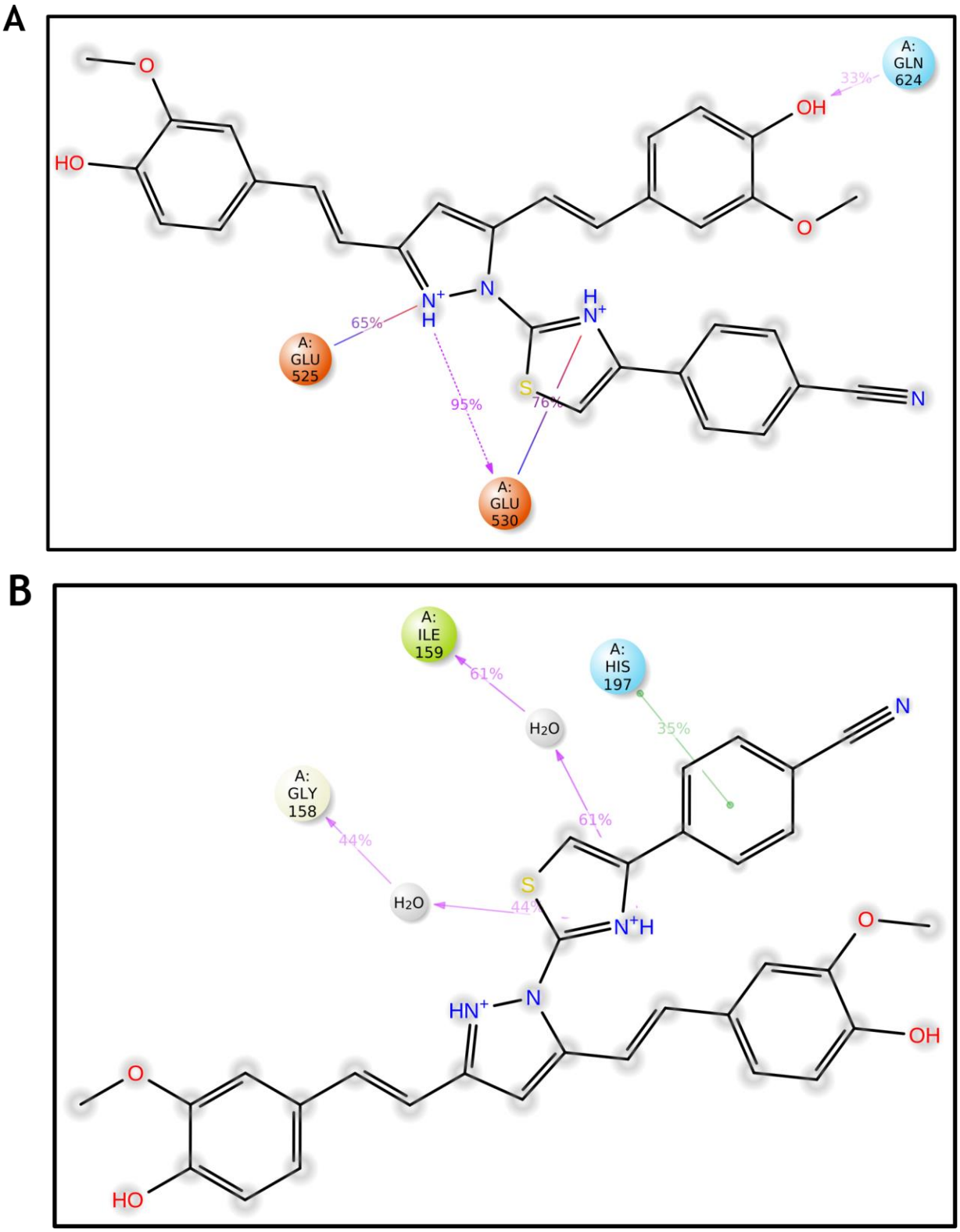

Figure 8: Ligand–atom interactions with the protein residues. (A) Protein MMP-2 and compound C2 and (B) Protein MMP-8 and compound C2.

A

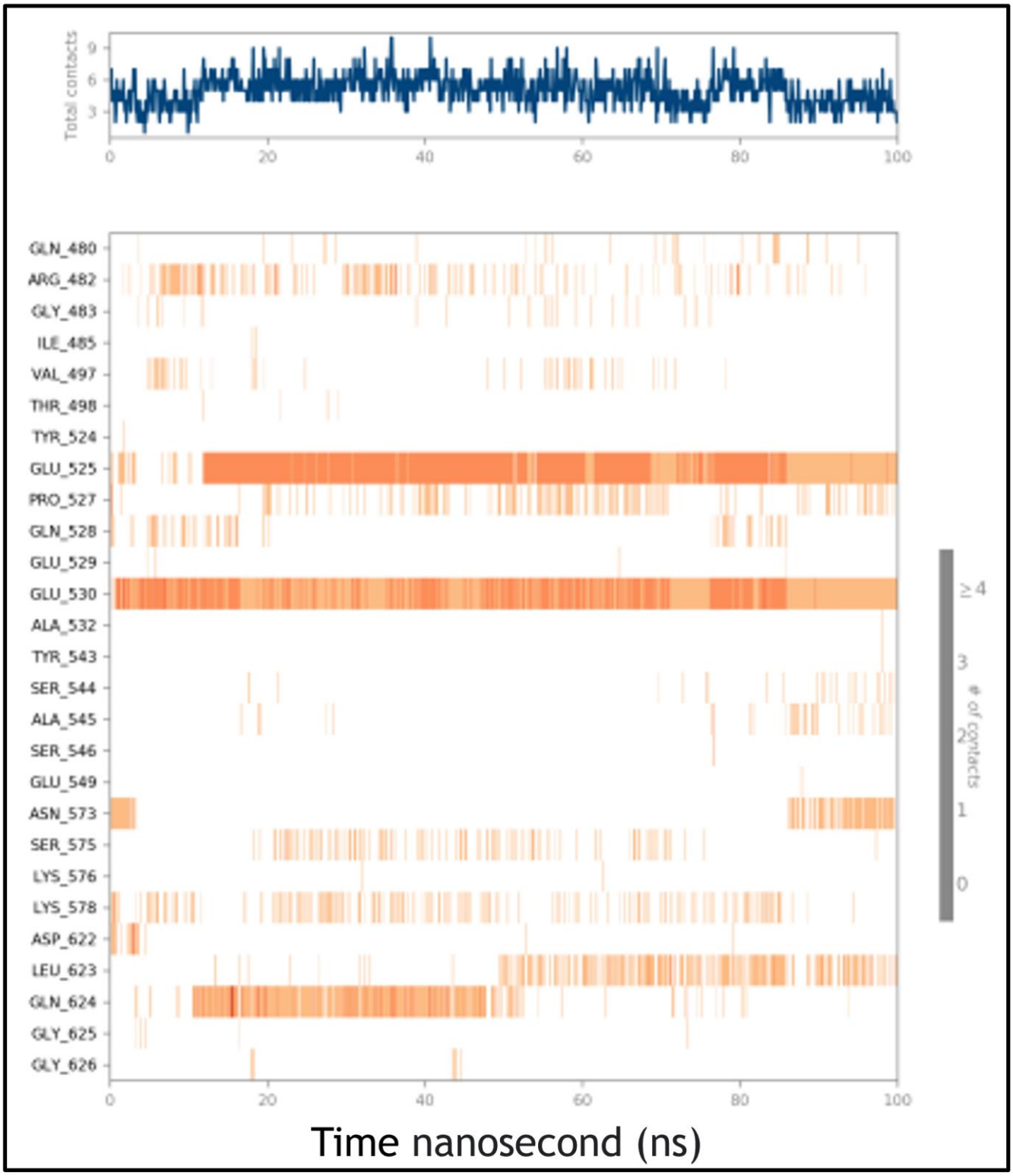
Total contacts
9
6
3
0
20
40
60
80
100
GLN_480
ARG_482
GLY_483
ILE_485
VAL_497
THR_498
TYR_524
GLU_525
PRO_527
GLN_528
GLU_529
GLU_530
ALA_532
TYR_543
SER_544
ALA_545
SER_546
GLU_549
ASN_573
SER_575
LYS_576
LYS_578
ASP_622
LEU_623
GLN_624
GLY_625
GLY_626
# of contacts
≥ 4
3
2
1
0
Time nanosecond (ns)

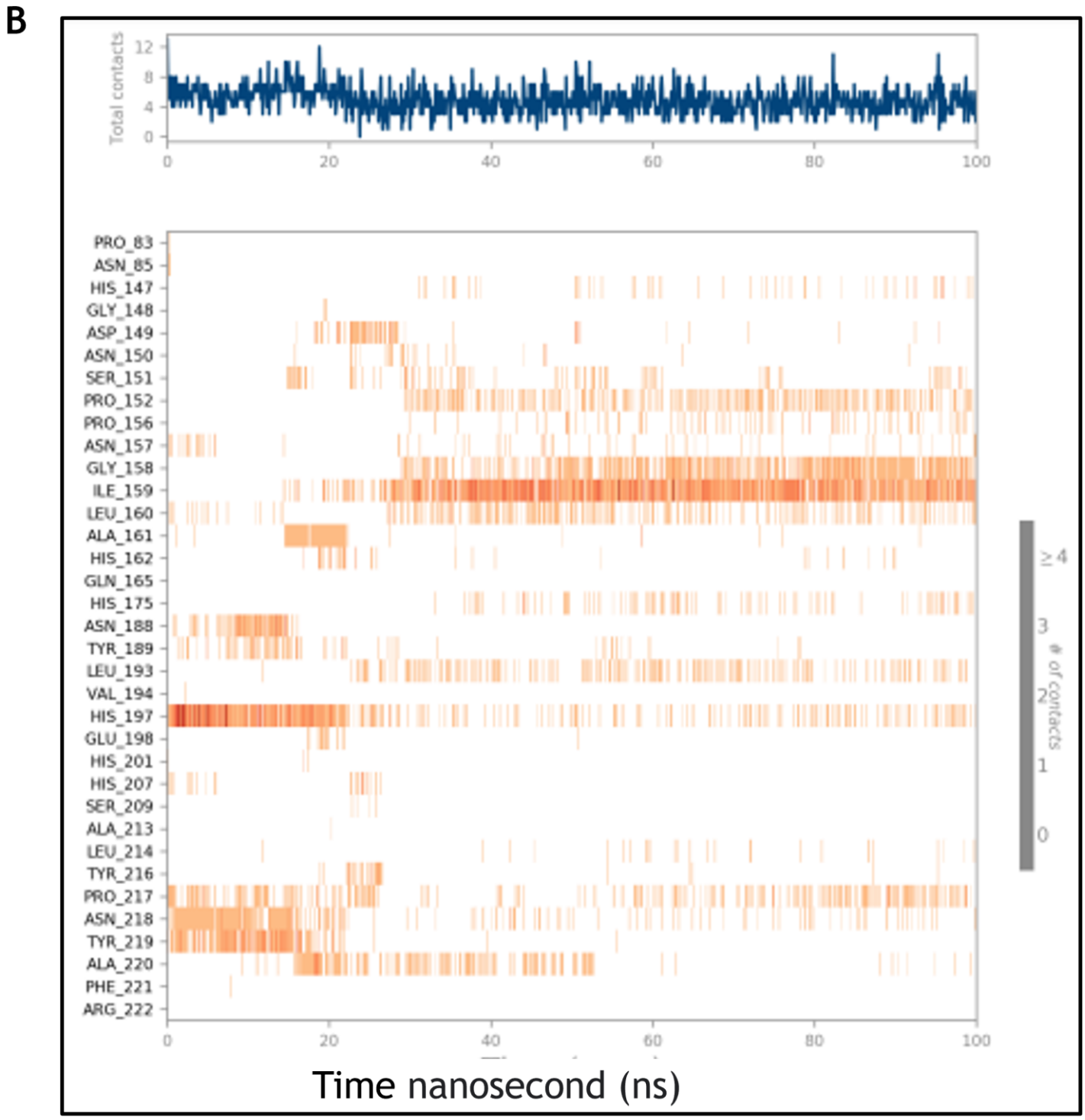

Figure 9: 2D diagram of interactions of Protein–ligand during 100 ns simulation period. (A) MMP-2/C2 complex and (B) MMP-8/C2 complex.

A

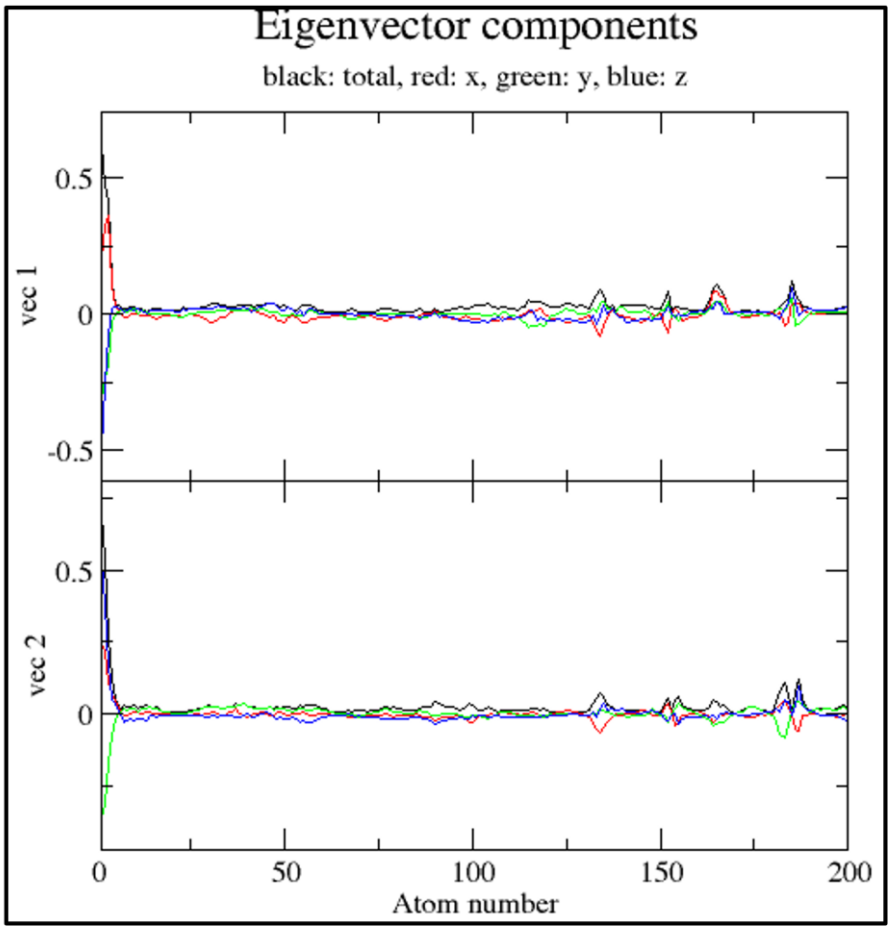
Eigenvector components
black: total, red: x, green: y, blue: z
vec 1
vec 2
0.5
0
-0.5
0
50
100
150
200
Atom number

B

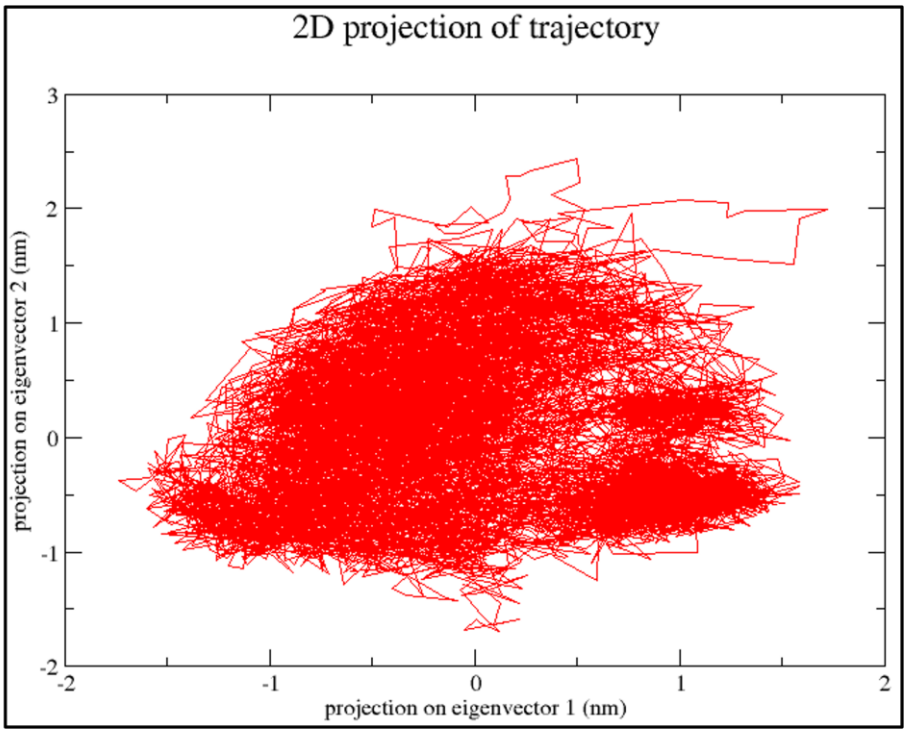
2D projection of trajectory
projection on eigenvector 2 (nm)
projection on eigenvector 1 (nm)
3
2
1
0
-1
-2
-2
-1
0
1
2

C

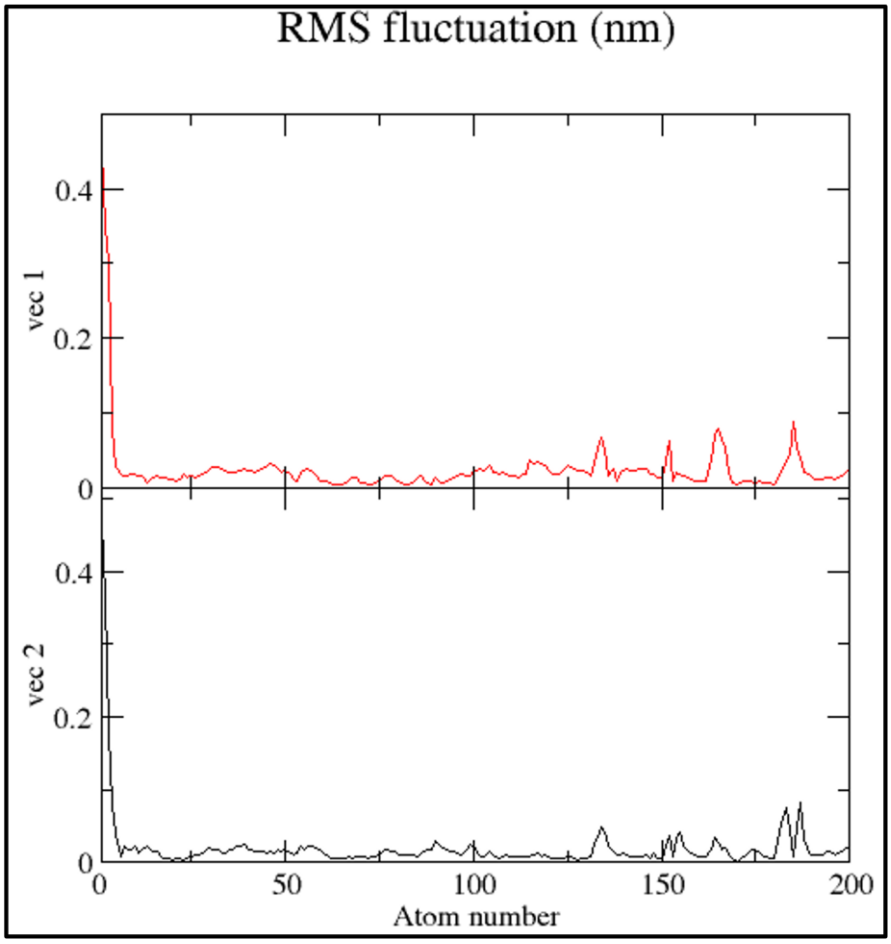
RMS fluctuation (nm)
vec 1
vec 2
0.4
0.2
0
0.4
0.2
0
0
50
100
150
200
Atom number

D

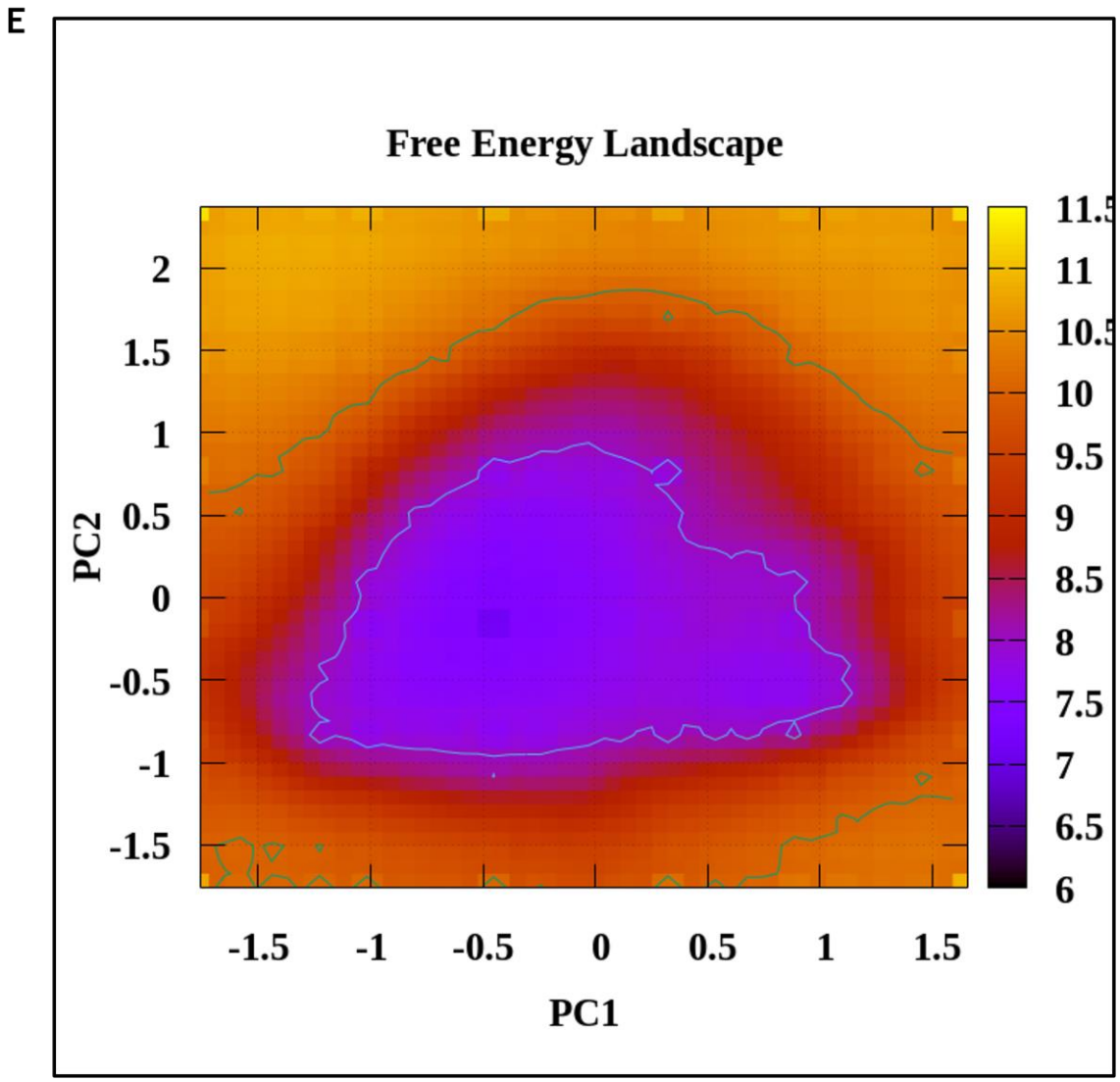

Figure 10. PCA-based confirmation of conformational alterations in MMP-2. (A) The eigenvalue plot generated from the MD trajectories and derived from the Cα covariance matrix. (B) MMP-2 protein principal component analysis. (C) The mobility plot of MMP-2 in modes 1 and 2 based on residues. (D) The MMP-2 protein's free energy profile. (E) Porcupine plots from the PCA analysis for PC1, showing how the Cα atoms moved and positioned themselves during the course of the 100 ns simulation.

A

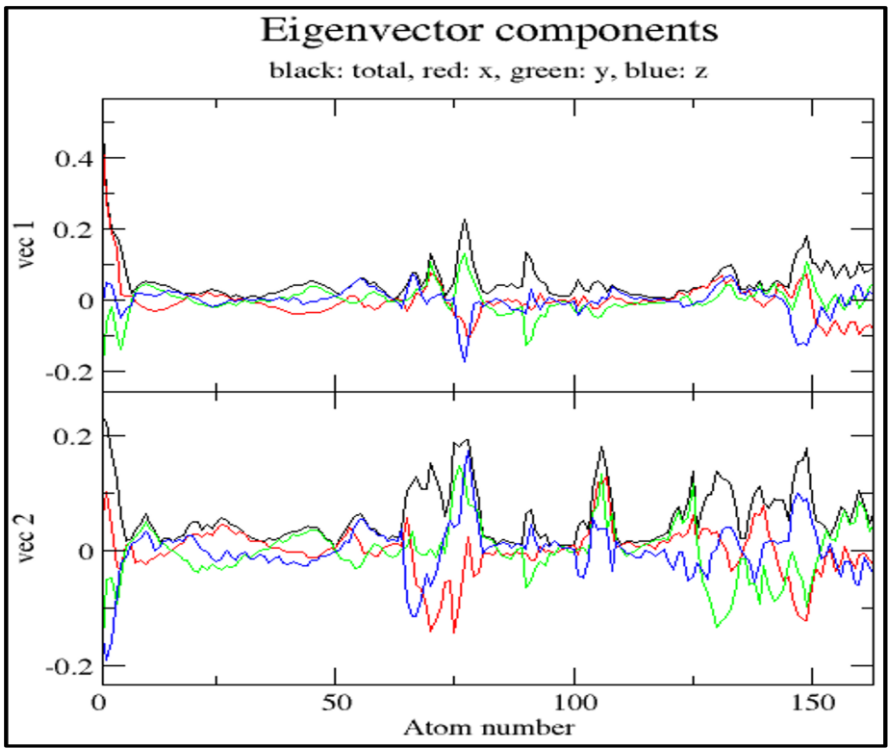
Eigenvector components
black: total, red: x, green: y, blue: z
vec 1
vec 2
0.4
0.2
0
-0.2
0.2
0
-0.2
0
50
100
150
Atom number

B

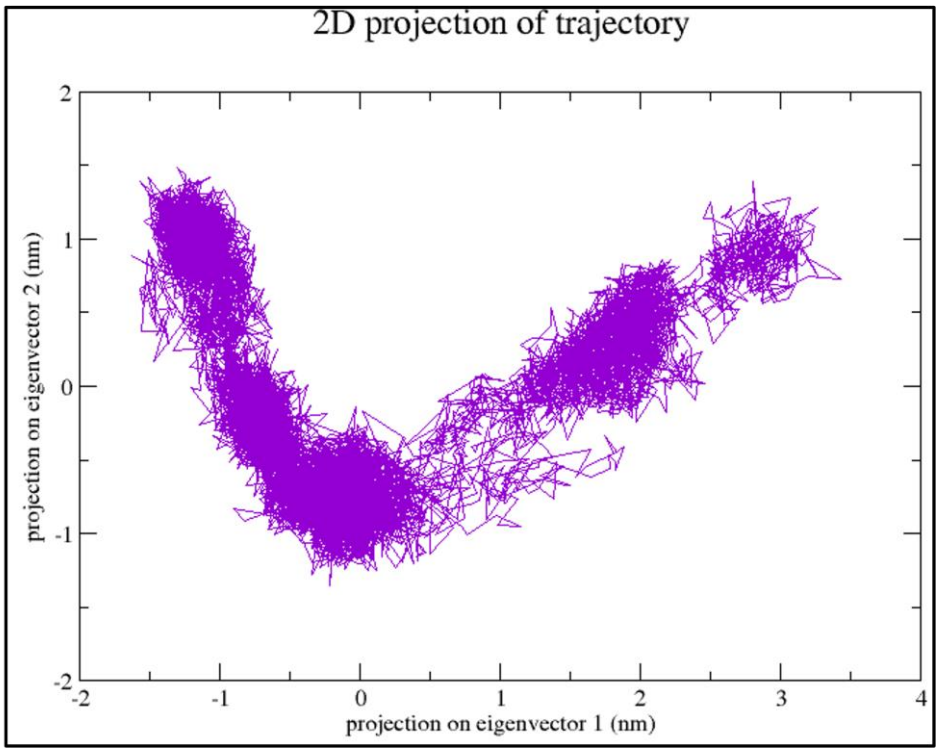
2D projection of trajectory
projection on eigenvector 2 (nm)
projection on eigenvector 1 (nm)
2
1
0
-1
-2
-2
-1
0
1
2
3
4

C

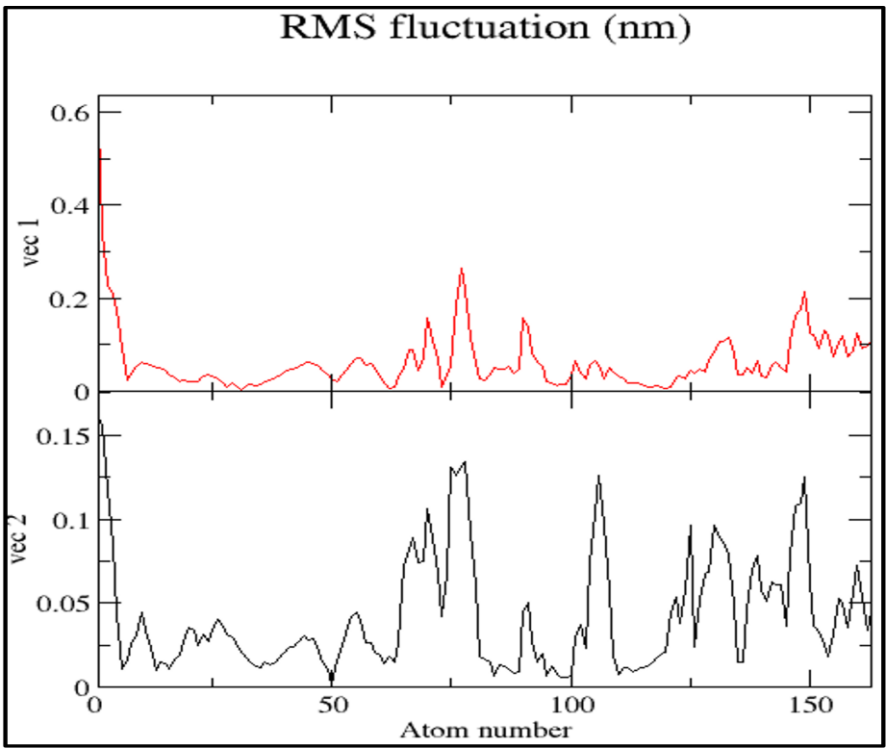
RMS fluctuation (nm)
vec 1
vec 2
0.6
0.4
0.2
0
0.15
0.1
0.05
0
0
50
100
150
Atom number

D

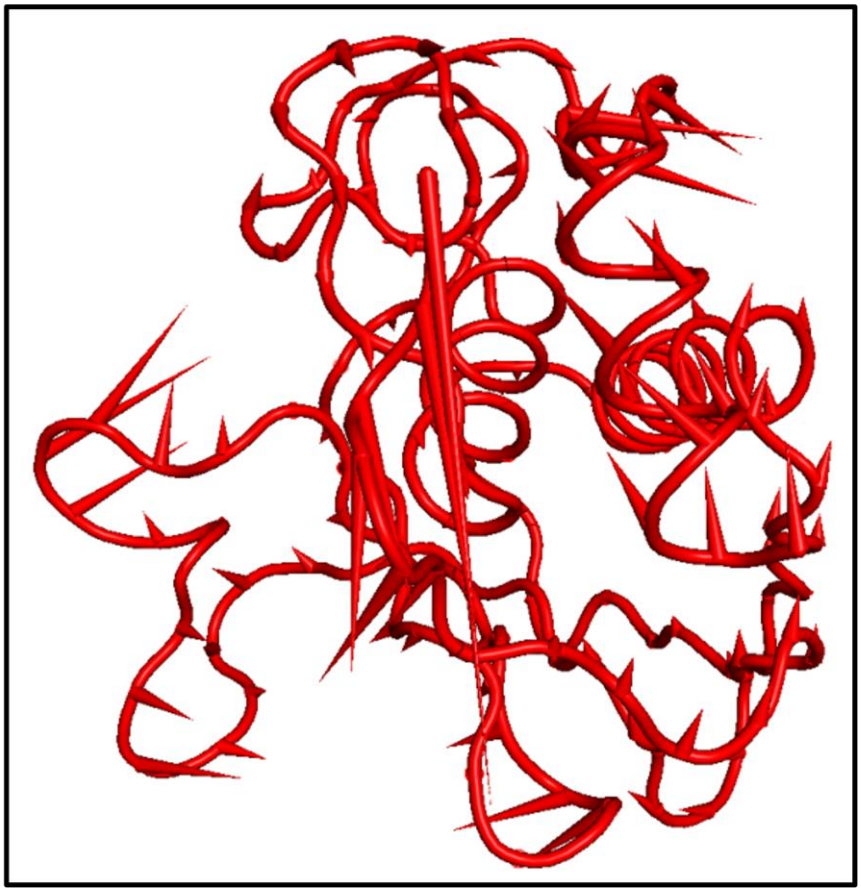

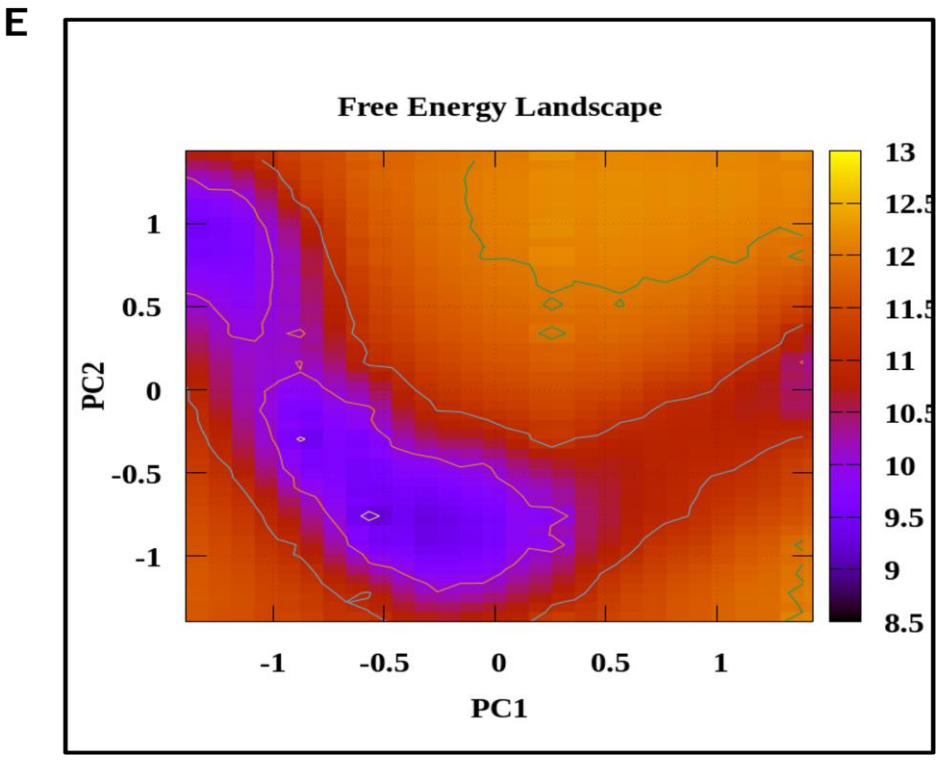

Figure 11. PCA-based confirmation of conformational alterations in MMP-8. (A) The eigenvalue plot generated from the MD trajectories and derived from the Cα covariance matrix. (B) MMP-8 protein principal component analysis. (C) The mobility plot of MMP-8 in modes 1 and 2 based on residues. (D) The MMP-8 protein's free energy profile. (E) Porcupine plots from the PCA analysis for PC1, showing how the Cα atoms moved and positioned themselves during the course of the 100 ns simulation.

Table 5. Binding free energies and energy components obtained by MM/GBSA (kcal/mol) during 100 ns MD simulation

Ligand-Protein complex	ΔGBind (Kcal/mol)	ΔGCoulomb (Kcal/mol)	ΔGHbond (Kcal/mol)	ΔGLipo (Kcal/mol)	ΔGPacking (Kcal/mol)	ΔGvdW (Kcal/mol)
C2/MMP-2 complex	-24.434	-25.7614	-1.097	-14.743	-0.147	-27.409
C2/MMP-8 complex	-12.347	-12.347	-0.279	-29.663	-3.086	-34.399

*Please take note that the table's abbreviations have the following meanings- *Coulomb :Coulomb energy; Hbond: Hydrogen-bonding correction. ;Packing: Pi-Pi packing correction; Lipo: Lipophilic energy; VdW: Van der Waals energy.

The molecular docking analysis was conducted using the CB Dock, a web-based online tools. The CB-Dock predicts the binding areas of a specific protein and determines the centers and diameters using a curvature-based cavity identification approach [20]. The compound was docked to predict C2 binding affinity against MMP-2 and MMP-8. Balogun et al., (2022) reported that the more negative the docking score, the greater the affinity [55]. The compound C2 showed higher binding and lower binding energy (-8.2 kcal/mol) compared to the reference gentamicin (-7.0 kcal/mol) indicated C2 are strongly bind in the active site of MMP-2 (Figure 3 and Table 3). Likewise, the compound C2 (-7.8 kcal/mol) showed lowest interaction energy and high binding affinity compared to gentamicin (-7.2 kcal/mol) in the active site of MMP-8 (Figure 4 and Table 4). From the Molecular docking findings can be predicted that compound C2 potentially binds the active site of the MMP-2 and MMP-8 and can regulate the activity and speed up the wound healing process.

The C2/MMP-2 complex had a RMSD below 3.0 Å, indicating stability. The ligand atoms fluctuated up to 9.7 Å before stabilizing, but the ligand RMSD did not significantly differ from the protein MMP-2 RMSD after stabilization (Figure 5A). Researchers claimed that the RMSD value up to 10 Å showed good stability [56]. the RMSF value for MMP-2/C2 complex was below 3 Å, indicating interaction stability (Figure 6A). The hydrogen bond interaction was attributed to Glu 530 and Gln 625 residues (Figure 7A and Figure 8A). The 2D diagram of the MMP-2-C2 complex showed a darker orange color, suggesting that the residues could bind the protein active site and potentially inhibit MMP-2 (Figure 9A). Furthermore, the C2/MMP-8 complex RMSD value showed stable binding in the active site of MMP-8, with RMSD values below 3.3 Å and 8.9 Å, respectively (Figure 5). The ligand RMSD fluctuated due to internal dynamics within the binding pocket. A similar study reported that a value of 10 Å has good stability [57]. The RMSF peaks indicate that the protein residues fluctuated most significantly throughout the simulation and are below that 3Å (Figure 6A). The protein-ligand contact involved eight hydrogen bond interactions, with the Asn 218 interaction being the highest (Figure. 7A). The 2D-interaction diagram showed four significant interaction types, making the complex stable (Figure 8A and Figure 9A).

The binding free energy of hit compound C2 with the MMP-2 and MMP-8 is calculated from 100 ns MD simulation trajectory and displays both complex binding free energy shift profiles (Table 4 and Table 5). The binding affinity of C2/MMP-2 (24.434 kcal/mol) is higher than C2/MMP-8 complex (−12.347 kcal/mol); however, both complexes showed higher negative free energy value. Prajapati et al. (2021) reported that a system is more stable if the free energy value is negative [25]. Tabti et al. (2023) reported that when the binding energy is lower (has a greater negative value), the related conformation and system are more stable [58]. Additionally, these energies directly affect the receptor-ligand complex's stability [25]. Our results indicated that the lead compound C2 satisfies the prime MM/GBSA approach to achieve a stable complex with MMP2 and MMP-8, and the energies predicted from the prime MM/GBSA are thermodynamically favorable. Notably, from the above data and discussion, it has been predicted that the proposed compound C2 possesses a strong binding affinity and stability toward MMP-2 compared to the MMP-8. Therefore, this study concludes that C2 could be a potential inhibitor of MMP-2. However, details of in vitro and in vivo studies are suggested for future testing and development as a therapeutic drug for wound healing.

In addition, we confirmed structural changes by using PCA to identify the protein's essential movements. The significant conformational variation between the first and final MD structures was identified using the PCA. Their disparate motion directions in relation to one another provided evidence for this. The higher displacements of some residues, which displayed two conformations and visited separate subspaces throughout the MD simulations, were confirmed by our study of the residue displacements based on the projection of the MD trajectories on the first and second components. This gave important insights into the structural variety of the bound and free states of the MMP-2 and MMP-8 proteins. The protein's stable structure and energy minima were intimately revealed by the free energy landscape (FEL) study. Two energy minima representing the two conformations of the protein (bound and unbound) for MMP-8 were found by FEL analysis of MMP-2 and MMP-8, whereas one energy minimum revealed the single conformation of the MMP-2 protein. Therefore, this study concludes that C2 could be a potential inhibitor of MMP-2. However, details of in vitro and in vivo studies are suggested for future testing and development as a therapeutic drug for wound healing.

5. Conclusions

The purpose of the current study was to investigate eight pyrazole-thiazole derivatives of curcumin as potential sources of wound healing medicine that target matrix metalloproteinases (MMPs), specifically MMP-2 and MMP-8 for wound healing. Thus, this study utilized computational approaches, including pharmacokinetics, ADMET prediction, molecular docking, MD simulation, and binding energy calculation from MD simulation trajectories. This study has identified one hit compound C2 based on the pharmacokinetic and ADMET-based evaluations and subjected it to molecular docking, MD simulation, and MMGBSA analysis. Based on their interaction energy, hydrogen, and hydrophobic bonding with the target protein, the molecular docking confirmed that C2 bound with targeted proteins MMP-2 and MMP-8. The molecular docking finding showed that compound C2 bound in the active site of MMP-3 with the lowest energy compared to MMP-8. The 100 ns MD simulation explored the dynamic nature of protein-ligand complexes. The 100ns MD simulation results suggested that C2/MMP-2 complex are more stable compared to the C2/MMP-8 complex. The PCA and FEL findings indicated that C2/MMP-2 complex are more stable compared to the C2/MMP-8 which consistent MMGBSA analysis. Notably, the binding free energy (ΔGBind) of C2 /MMP-2 complexes was the highest (ΔGBind: -24.434 kcal/mol), indicating the most significant binding affinity. In light of our findings, the identified C2 compound exhibit remarkable potential to inhibit MMP-2 compared to MMP-8. Therefore, C2 might be considered for further *in vitro*, *in vivo*, and clinical trials analysis to demonstrate their true efficacy, and considerably more work will need to be done to determine the compound C2 as MMP-2 inhibitor.

Acknowledgement

The authors are grateful to the Ministry of Higher Education , Malaysia for giving the funding under the Fundamental Research Grant Scheme (FRGS) No. FRGS/1/2021/STG05/UMP/02/6 (University Reference-RDU210133) and Universiti Malaysia Pahang for providing laboratory facilities, as well as additional funding under Postgraduate Research Grants Scheme (PGRS) Grant (University reference -PGRS220353).

Disclosure statement

The authors have no conflict of interest.

References

[1] N.X. Landén, D. Li, and M. Ståhle. (2016). Transition from inflammation to proliferation: a critical step during wound healing. Cellular and Molecular Life Sciences. 73 3861-3885.

[2] F. Zakaria, N.N.M. Anuar, N.S.N. Hisam, J.K. Tan, F. Zakaria, S.M.M. Fauzi, S.E. Ashari. (2023). An investigation of the in vitro wound healing potential of Mitragyna speciosa (Korth.) Havil leaf ultrasound-assisted methanol crude extract and fractions. Biocatalysis and Agricultural Biotechnology. 102707.

[3] A. Balachandran, S.B. Choi, M.M. Beata, J. Małgorzata, G.R. Froemming, C.A. Lavilla Jr, P.N. Okechukwu. (2023). Antioxidant, Wound Healing Potential and In Silico Assessment of Naringin, Eicosane and Octacosane. Molecules. 28 (3) 1043.

[4] V.P. Nakhate, N.S. Akojwar, S.K. Sinha, A.D. Lomte, M. Dhobi, P.R. Itankar, S.K. Prasad. (2023). Wound healing potential of Acacia catechu in streptozotocin-induced diabetic mice using in vivo and in silico approach. Journal of Traditional and Complementary Medicine. 13 (5) 489-499.

[5] A.Y.M. Alabdali, R. Khalid, M. Kzar, M.O. Ezzat, G.M. Huei, T.W. Hsia, S.I. Khalivulla. (2022). Design, synthesis, in silico and antibacterial evaluation of curcumin derivatives loaded nanofiber as potential wound healing agents. Journal of King Saud University-Science. 34 (7) 102205.

[6] D. Rathee, V. Lather, A.S. Grewal, H. Dureja. (2018). Targeting matrix metalloproteinases with novel diazepine substituted cinnamic acid derivatives: design, synthesis, in vitro and in silico studies. Chemistry Central Journal. 12 (1) 1-15.

[7] V.R. Krishnaswamy, D. Mintz, I. Sagi. (2017). Matrix metalloproteinases: The sculptors of chronic cutaneous wounds. Biochimica et Biophysica Acta (BBA)-Molecular Cell Research. 1864 (11) 2220-2227.

[8] M. Kandhwal, T. Behl, S. Singh, N. Sharma, S. Arora, S. Bhatia, S. Bungau. (2022). Role of matrix metalloproteinase in wound healing. American Journal of Translational Research. 14 (7) 4391.

[9] A. Nikolov, N. Popovski. (2021). Role of gelatinases MMP-2 and MMP-9 in healthy and complicated pregnancy and their future potential as preeclampsia biomarkers. Diagnostics. 11 (3) 480.

[10] M.P. Caley, V.L. Martins, E.A. O'Toole. (2015). Metalloproteinases and wound healing. Advances in wound care. 4 (4) 225-234.

[11] P.K. Gajendrareddy, C.G. Engeland, R. Junges, M.P. Horan, I.G. Rojas, P.T. Marucha. (2013). MMP-8 overexpression and persistence of neutrophils relate to stress-impaired healing and poor collagen architecture in mice. Brain, behavior, and immunity. 28 44-48.

[12] B. Amato, G. Coretti, R. Compagna, M. Amato, G. Buffone, D. Gigliotti, S. de Franciscis. (2015). Role of matrix metalloproteinases in non-healing venous ulcers. International Wound Journal. 12 (6) 641-645.

[13] K. Chowdhury, A. Sharma, T. Sharma, S. Kumar, C.C. Mandal. (2017). Simvastatin and MBCD inhibit breast cancer-induced osteoclast activity by targeting osteoclastogenic factors. Cancer investigation. 35 (6) 403-413.

[14] M.A. Tomeh, R. Hadianamrei, X. Zhao. (2019). A review of curcumin and its derivatives as anticancer agents. International journal of molecular sciences. 20 (5) 1033.

[15] R. Palabindela, R. Guda, G. Ramesh, R. Bodapati, S.K. Nukala, P. Myadaraveni, M. Kasula. (2023). Curcumin based pyrazole-thiazole hybrids as antiproliferative agents: Synthesis, pharmacokinetic, photophysical properties, and docking studies. Journal of Molecular Structure. 1275 134633.

[16] K. Bairwa, J. Grover, M. Kania, S.M. Jachak. (2014). Recent developments in chemistry and biology of curcumin analogues. RSC advances. 4 (27) 13946-13978.

[17] F. Farhat, S.S. Sohail, F. Siddiqui, R.R. Irshad, D. Ø. Madsen. (2023). Curcumin in wound healing—A bibliometric analysis. Life. 13 (1) 143.

[18] Lipinski, A. Christopher. (2004). Lead-and drug-like compounds: the rule-of-five revolution. Drug discovery today: Technologies 1 (4) 337-341.

[19] M. Roney, A.R. Issahaku, M.S. Forid, A.K.M. Huq, M.E. Soliman, M.F.F. Mohd Aluwi, S.N. Tajuddin. (2023). In silico evaluation of usnic acid derivatives to discover potential antibacterial drugs against DNA gyrase B and DNA topoisomerase IV. Journal of Biomolecular Structure and Dynamics. 41 (24) 1-10.

[20] S. Ekins, J. Mestres, B. Testa. (2007). *In silico* pharmacology for drug discovery: methods for virtual ligand screening and profiling. British journal of pharmacology. 152 (1) 9-20.

[21] D.E. Pires, T.L. Blundell, D.B. Ascher. (2015). pkCSM: predicting small-molecule pharmacokinetic and toxicity properties using graph-based signatures. Journal of medicinal chemistry. 58 (9) 4066-4072.

[22] Y. Liu, M. Grimm, W.T. Dai, M.C. Hou, Z.X. Xiao, Y. Cao. (2020). CB-Dock: A web server for cavity detection-guided protein–ligand blind docking. Acta Pharmacologica Sinica. 41 (1) 138-144.

[23] A.M. Huq, M. Roney, S. Imran, S.U. Khan, S. M.N. Uddin, T.T. Htar, S.N. Tajuddin. (2023). Virtual screening of bioactive anti-SARS-CoV natural products and identification of 3β, 12-diacetoxyabieta-6, 8, 11, 13-tetraene as a potential inhibitor of SARS-CoV-2 virus and its infection related pathways by MD simulation and network pharmacology. Journal of Biomolecular Structure and Dynamics. 41 (23) 1-14.

[24] M.H.S Abuthakir, M.A. Al-Dosary, A.A. Hatamleh, H.A. Alodaini, P. Perumal, M. Jeyam. (2022). Platyphylloside, a potential inhibitor from epicarp of B. aegyptiaca against CYP450 protein in T. rubrum–In vitro and in silico approaches. Saudi Journal of Biological Sciences. 29 (5) 3899-3910.

[25] J. Prajapati, R. Patel, D. Goswami, M. Saraf, R.M. Rawal. (2021). Sterenin M as a potential inhibitor of SARS-CoV-2 main protease identified from MeFSAT database using molecular docking, molecular dynamics simulation and binding free energy calculation. Computers in Biology and Medicine. 135 104568.

[26] D.C. Patel, K.R. Hausman, M. Arba, A. Tran, P.M. Lakernick, C. Wu. (2022). Novel inhibitors to ADP ribose phosphatase of SARS-CoV-2 identified by structure-based high throughput virtual screening and molecular dynamics simulations. Computers in Biology and Medicine. 140 105084.

[27] G.M. Basha, R.S. Parulekar, A.G. Al-Sehemi, M. Pannipara, V. Siddaiah, S. Kumari, P.B. Choudhari, Y. Tamboli. (2022). Design and in silico investigation of novel Maraviroc analogues as dual inhibition of CCR-5/SARS-CoV-2 Mpro. Journal of Biomolecular Structure and Dynamics. 40 (21) 11095-110.

[28] A. Amadei, A.B. Linssen, H.J. Berendsen. (1993). Essential dynamics of proteins. Proteins Struct Proteins. 17 (4) 412–425.

[29] Z.T. Muhseen, G. Li. (2019). Promising terpenes as natural antagonists of cancer: an in-silico approach. Molecules. 25 (1) 155.

[30] T. Ichiye, M. Karplus. (1991). Collective motions in proteins: A covariance analysis of atomic fluctuations in molecular dynamics and normal mode simulations. Proteins: Structure, Function, and Bioinformatics. 11 205–217.

[31] A.E. García. (1992). Large-amplitude nonlinear motions in proteins. Physical review letters. 68 (17) 2696.

[32] A.K. Singh, P.P. Kushwaha, K.S. Prajapati, M. Shuaib, S. Gupta, S. Kumar (2021). Identification of FDA approved drugs and nucleoside analogues as potential SARS-CoV-2 A1pp domain inhibitor: An in silico study. Computers in Biology and Medicine. 130 104185.

[33] S. Gupta, A.K. Singh, P.P. Kushwaha, K.S. Prajapati, M. Shuaib, S. Senapati, S. Kumar. (2021). Identification of potential natural inhibitors of SARS-CoV2 main protease by molecular docking and simulation studies. Journal of Biomolecular Structure and Dynamics. 39 (12) 4334-45.

[34] N. Baruah, M. Das, K.K. Saikia. (2023). GC-MS analysis, molecular docking with Human TGF-β Receptor I, and the prediction of pharmacokinetic properties of active compounds isolated from Musa balbisiana Colla fruit pulp extracts. International Journal of Chemical and Biochemical Sciences. 24 (6) 184-194.

[35] S. Bendjedid, & D. Benouchenne. (2023). In silico studies for assessing physicochemical, pharmacokinetic and cytotoxicity properties of bioactive molecules identified by LC-MS in Aloe vera leaves extracts. South African Journal of Botany. 157 75-81.

[36] X. Chen, H. Li, L. Tian, Q. Li, J. Luo, Y. Zhang. (2020). Analysis of the physicochemical properties of acaricides based on Lipinski's rule of five. Journal of computational biology. 27 (9) 1397-1406.

[37] B. Shaker, S. Ahmad, J. Lee, C. Jung, D. Na. (2021). In silico methods and tools for drug discovery. Computers in biology and medicine. 137 104851.

[38] P. Ojuka, N.M. Kimani, S. Apollo, J. Nyariki, R.S. Ramos, C.B. Santos. (2023). Phytochemistry of the Vepris genus plants: A review and in silico analysis of their ADMET properties. South African Journal of Botany. 157 106-114.

[39] G. Moroy, V.Y. Martiny, P. Vayer, B.O. Villoutreix, M.A. Miteva (2012). Toward in silico structure-based ADMET prediction in drug discovery. Drug discovery today. 17 (1-2) 44-55.

[40] M. Roney, A.M. Huq, K. Rullah, H.A. Hamid, S. Imran, M.A. Islam, M.F.F. Mohd Aluwi. (2021). Virtual screening-based identification of potent DENV-3 RdRp protease inhibitors via in-house usnic acid derivative database. Journal of

Computational Biophysics and Chemistry. 20 (08) 797-814.

[41] A.K. Padhi, A. Seal, J.M. Khan, M. Ahamed, T. Tripathi. (2021). Unraveling the mechanism of arbidol binding and inhibition of SARS-CoV-2: Insights from atomistic simulations. European journal of pharmacology. 894 173836.

[42] S. Bhowmick, S.A. Alissa, S.M. Wabaidur, R.V. Chikhale, M.A. Islam. (2020). Structure-guided screening of chemical database to identify NS3-NS2B inhibitors for effective therapeutic application in dengue infection. Journal of Molecular Recognition. 33 (7) e2838.

[43] M. De Vivo, M. Masetti, G. Bottegoni, A. Cavalli. (2016). Role of molecular dynamics and related methods in drug discovery. Journal of medicinal chemistry. 59 (9) 4035-4061.

[44] S. Kumar, G. Subramaniam, K. Karuppanan. (2023). Human monkeypox outbreak in 2022. Journal of Medical Virology. 95 (1) e27894.

[45] B. Rashidieh, M. Molakarimi, A. Mohseni, S.M. Tria, H. Truong, S. Srihari, R.C. Adams, M. Jones, P.H. Duijf, M. Kalimutho. (2021). Targeting BRF2 in cancer using repurposed drugs. Cancers. 13 (15) 3778.

[46] T. Wang, W. Yi, Y. Zhang, H. Wu, H. Fan, J. Zhao, S. Wang (2023). Sodium alginate hydrogel containing platelet-rich plasma for wound healing. Colloids and Surfaces B: Biointerfaces. 222 113096.

[47] C. Khoswanto. (2023). Role of matrix metalloproteinases in bone regeneration: Narrative review. Journal of Oral Biology and Craniofacial Research. 13 (5) 539-543.

[48] M.S. Azuri, M.S. Forid, W.M.W. Ishak, N.A.A Azhar. (2023). Optimization of Chitosan Concentration on Physicochemical Properties of Polyvinyl Alcohol-Based Hydrogel. International Journal of Chemical and Biochemical Science. 24 (8) 147-157.

[49] L. Zheng, K. Amano, K. Iohara, M. Ito, K. Imabayashi, T. Into, M. Nakashima. (2009). Matrix metalloproteinase-3 accelerates wound healing following dental pulp injury. The American journal of pathology. 175 (5) 1905-1914.

[50] M.S. Criollo-Mendoza, L.S. Contreras-Angulo, N. Leyva-López, E.P. Gutiérrez-Grijalva, L.A. Jiménez-Ortega, J.B. Heredia. (2023). Wound healing properties of natural products: Mechanisms of action. Molecules. 28 (2) 598.

[51] A. Kumari, N. Raina, A. Wahi, K.W. Goh, P. Sharma, R. Nagpal, M. Gupta. (2022). Wound-Healing Effects of Curcumin and Its Nanoformulations: A Comprehensive Review. Pharmaceutics. 14 (11) 2288.

[52] A. Sood, A. Dev, S.S. Das, H.J. Kim, A. Kumar, V.K. Thakur, S.S. Han. (2023). Curcumin-loaded alginate hydrogels for cancer therapy and wound healing applications: A review. International Journal of Biological Macromolecules. 123283.

[53] D. Rajaraman, L.A. Anthony, P. Nethaji, R. Vallangi (2023). One-pot synthesis, NMR, quantum chemical approach, molecular docking studies, drug-likeness and in-silico ADMET prediction of novel 1-(2, 3-dihydrobenzo [b][1, 4] dioxin-6-yl)-2-(furan-2-yl)-4, 5-diphenyl-1H-imidazole derivatives. Journal of Molecular Structure. 1273 134314.

[54] D.A. Omoboyowa, M.N. Iqbal, T.A. Balogun, D.S. Bodun, J.O. Fatoki, O.E. Oyeneyin. (2022). Inhibitory potential of phytochemicals from Chromolaena odorata L. against apoptosis signal-regulatory kinase 1: A computational model against colorectal cancer. Computational Toxicology. 23 100235.

[55] T.A. Balogun, M.N. Iqbal, O.A. Saibu, M.O. Akintubosun, O.M. Lateef, U.C. Nneka, O.T. Abdullateef, D.A. Omoboyowa. (2022). Discovery of potential HER2 inhibitors from Mangifera indica for the treatment of HER2-Positive breast cancer: an integrated computational approach. Journal of Biomolecular Structure and Dynamics. 40 (23) 12772-12784.

[56] M.A.S Khan, M.I. Miah, Z. Islam, S. Afrin, M.F. Ahmed, S.R. Rahman. (2023). Molecular docking and dynamics simulation study of medicinal fungi derived secondary metabolites as potential inhibitor for COVID-19 treatment. Informatics in Medicine Unlocked. 41 101305.

[57] M. Waqas, S.A. Halim, A. Ullah, A.A.M. Ali, A. Khalid, A.N. Abdalla, A. Al-Harrasi (2023). Multi-Fold Computational Analysis to Discover Novel Putative Inhibitors of Isethionate Sulfite-Lyase (Isla) from Bilophila wadsworthia: Combating Colorectal Cancer and Inflammatory Bowel Diseases. Cancers. 15 (3) 901.

[58] K. Tabti, I. Ahmad, I. Zafar, A. Sbai, H. Maghat, M. Bouachrine, T. Lakhlifi (2023). Profiling the structural determinants of pyrrolidine derivative as gelatinases (MMP-2 and MMP-9) inhibitors using in silico approaches. Computational Biology and Chemistry. 104 107855.